Technical Report CHL-99-1
March 1999

US Army Corps of Engineers
Waterways Experiment Station

Coastal Inlets Research Program

Ponce de Leon Inlet, Florida, Site Investigation

Report 2
Inlet Hydrodynamics: Monitoring and Interpretation of Physical Processes

by Gary A. Zarillo, Florida Institute of Technology
Adele Militello, WES

Prepared for Headquarters, U.S. Army Corps of Engineers

The contents of this report are not to be used for advertising, publication, or promotional purposes. Citation of trade names does not constitute an official endorsement or approval of the use of such commercial products.

The findings of this report are not to be construed as an official Department of the Army position, unless so designated by other authorized documents.

Coastal Inlets Research Program

Technical Report CHL-99-1
March 1999

Ponce de Leon Inlet, Florida, Site Investigation

Report 2
Inlet Hydrodynamics: Monitoring and Interpretation of Physical Processes

by Gary A. Zarillo

Division of Marine and Environmental Systems
Florida Institute of Technology
150 W. University Boulevard
Melbourne, FL 32901

Adele Militello

U.S. Army Corps of Engineers
Waterways Experiment Station
3909 Halls Ferry Road
Vicksburg, MS 39180

Report 2 of a series

Approved for public release; distribution is unlimited

Prepared for U.S. Army Corps of Engineers
Washington, DC 20314-1000

Under CIRP Inlet Modeling System WU 32934

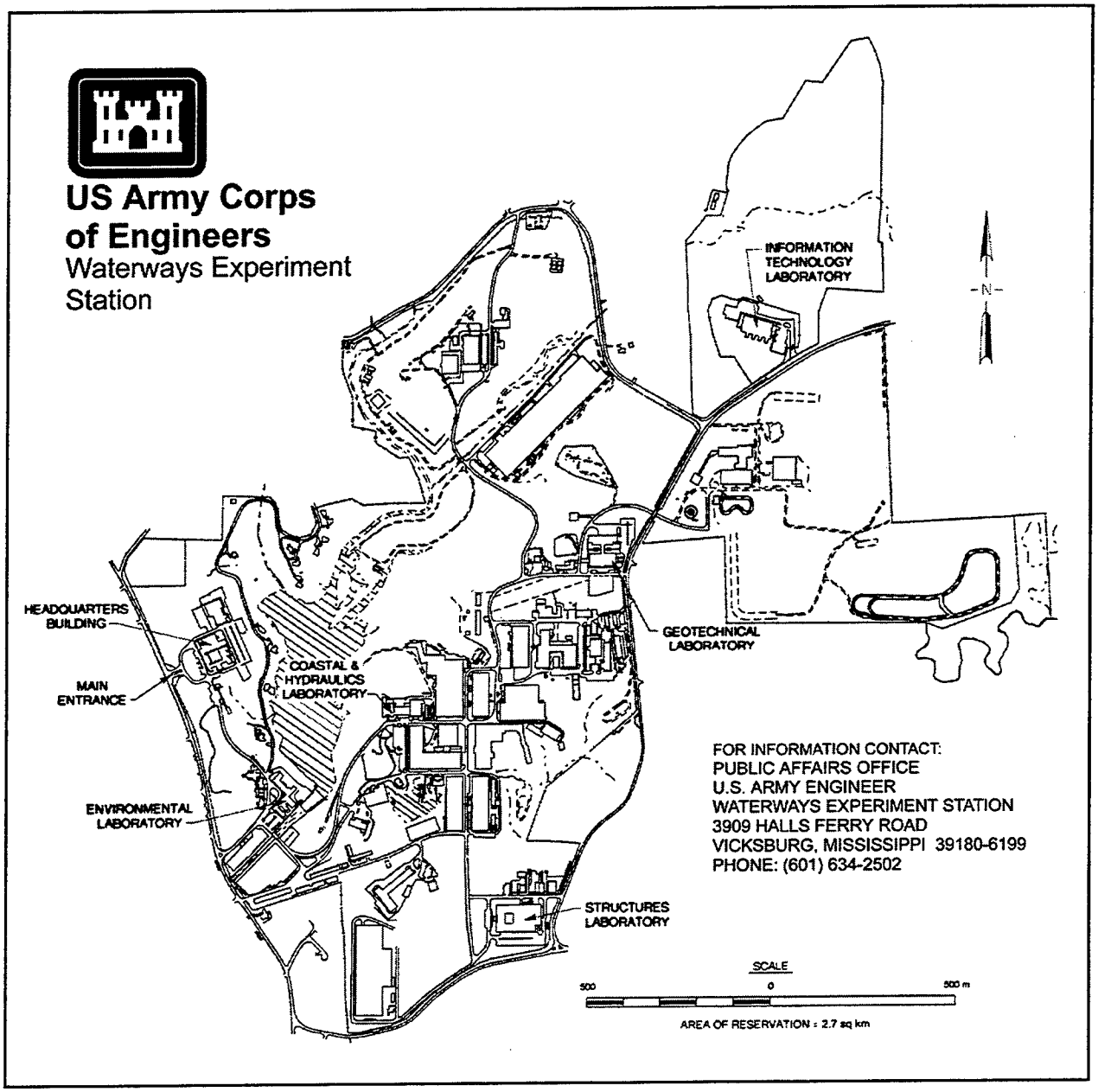

Waterways Experiment Station Cataloging-in-Publication Data

Zarillo, Gary A.

Ponce de Leon Inlet, Florida site investigation. Report 2, Inlet hydrodynamics : monitoring and interpretation of physical processes / by Gary A. Zarillo, Adele Militello ; prepared for U.S. Army Corps of Engineers.

39 p. : ill. ; 28 cm. — (Technical report ; CHL-99-1 rept.2)

Includes bibliographic references.

1. Ocean waves — Measurement. 2. Wind waves — Measurement. 3. Inlets — Florida. 4. Ponce de Leon Inlet (Fla.) I. Militello, Adele. II. United States. Army. Corps of Engineers. III. U.S. Army Engineer Waterways Experiment Station. IV. Coastal and Hydraulics Laboratory (U.S. Army Engineer Waterways Experiment Station) V. Title. VI. Series: Technical report (U.S. Army Engineer Waterways Experiment Station) ; CHL-99-1 rept.2.

TA7 W34 no.CHL-99-1 rept.2

Contents

Preface vi

Conversion Factors, Non-SI to SI Units of Measurement vii

1 Introduction and Goals 1

2 Overview of Inlet Processes and Study Site 4

Inlet Processes 4
Site Description 5

3 Project Tasks and Methods 7

Logistics and Marine Operations 7
Measurement of Waves, Currents, and Water Level 7
Data Analysis Methods 9
Data Archiving 9

4 Site Investigation Results 11

Data Return 11
Wave Statistics and Spectra 11
Tidal and Subtidal Motion 16
Tidal Harmonics and Spectra 27

5 Conclusions 30

References 32

Appendix A: Tidal-Constituent Amplitudes for Water Level at the Six Instrument Locations A1

Appendix B: Conversion Table for Calendar Day and Julian Day B1

SF 298

List of Figures

Figure 1. Ponce Inlet study area and location of monitoring stations 2

Figure 2. Schematic view of sensor package 8

Figure 3. Significant wave height and peak period at Station A 12

Figure 4. Significant wave height and peak direction at Station A 12

Figure 5. Significant wave height and peak period at Station B 13

Figure 6. Significant wave height and peak period at Station C 13

Figure 7. Significant wave height at Stations A, B, and C 14

Figure 8. Spectra of wave height for Stations A, B, and C at 2130 on 4 September 1997 14

Figure 9. Spectra of wave height for Stations A, B, and C at 2130 on 24 August 1997 15

Figure 10. Comparison of lower and higher wave-energy spectra at Station A 15

Figure 11. Comparison of lower wave-energy spectra at Stations A, B, and C at 0330 on 13 September 1997 16

Figure 12. Time series of water level at Station A 17

Figure 13. Time series of current speed and direction at Station A 17

Figure 14. Time series of current and water level at Station A 18

Figure 15. Time series of water level at Station B from 22 August to 1 October 1997 18

Figure 16. Time series of current speed and direction at Station B 19

Figure 17. Time series of water level at Station C from 22 August to 1 October 1997 19

Figure 18. Time series of current speed and direction at Station C 20

Figure 19. Time series of water level at Stations B and C 20

Figure 20. Time series of water elevation at Station D 21

Figure 21. Time series of current speed and direction at Station D 21

Figure 22. Time series of water level at Station E 22

Figure 23. Time series of current speed and direction at Station E 23

Figure 24. Time series of water level at Station F 23

Figure 25. Time series of current speed and direction at Station F 24

Figure 26. Tidal elevations at Stations D, E, and F from 12 October to 17 October 1997 24

Figure 27. Time series of low-pass filtered water level at Stations A and D and current speed at Station D 25

Figure 28. Time series of low-pass filtered water level and current speed at Station D 26

Figure 29. Time series low-pass filtered water level at Stations D and F and current at Station F 26

Figure 30. Time series of low-pass filtered water level at back-bay monitoring stations 27

Figure 31. Energy spectrum of water level at Station D 29

Figure 32. Energy spectrum of water level at Station E 29

Figure 33. Energy spectrum of water level at Station F 29

Preface

The study described herein was performed as part of the activities of the Coastal Inlets Research Project (CIRP), which is being conducted at the U.S. Army Engineer Waterways Experiment Station (WES), Coastal and Hydraulics Laboratory (CHL). The work was performed under CIRP Work Unit 32934 "Inlet Modeling System" (IMS) and supported in part by CIRP Work Unit 32929 "Inlet Channels and Shorelines." The CIRP Program Manager and Technical Leader were Mr. E. Clark McNair, Jr., CHL, and Dr. Nicholas C. Kraus, Coastal Sediments and Engineering Division (CC), CHL, respectively. The Headquarters, U.S. Army Corps of Engineers, Technical Monitors of the CIRP Program were Messrs. John P. Bianco, Barry W. Holliday, and Charles B. Chesnutt.

During the planning and data-collection period, Dr. Jane M. Smith, Coastal Processes Branch (CP), CC, was the Principal Investigator (PI) of the IMS Work Unit, and Ms. Julie Rosati, CP, was the PI of the Inlet Channels and Shorelines Work Unit. In October 1998, Dr. Adele Militello, Coastal Hydrodynamics Branch, Navigation and Harbors Division (CN), CHL, became the PI of the IMS Work Unit. This report was prepared by Dr. Gary A. Zarillo of the Florida Institute of Technology (FIT) and Dr. Militello. Technical review was provided by Ms. Rosati and Dr. Kraus.

CHL personnel who participated in the field effort were Dr. Smith, Dr. Militello, Dr. Kraus, and Mr. Tim Welp, Prototype Measurement and Analysis Branch, CC.

Other personnel associated with the FIT made substantial contributions to the data collection and analysis effort. Mr. Douglas Chapman designed and built the instrument packages. Mr. Richard Gurlek captained the research vessel during instrument deployment and retrieval. Mr. Clement R. Surak assisted in analysis and quality control of the data. Mr. Kenneth Connell and Ms. Michelle Peters provided logistical support and coordination assistance in the field effort.

This study was performed under the general supervision of Dr. James R. Houston and Mr. Charles C. Calhoun Jr. (retired), Director and Assistant Director, respectively, CHL. Direct supervision of this project was provided by Mr. Thomas W. Richardson, Chief of CC, and by Mr. Claude E. Chatham, Chief of CN.

At the time of publication of this report, Acting Director of WES was COL Robin R. Cababa, EN.

Conversion Factors, Non-SI to SI Units of Measurement

Non-SI units of measurement used in this report can be converted to SI units as follows:

Multiply	By	To Obtain
degree (angle)	0.01745329	radians
feet	0.3048	meters
pounds (mass)	0.4545924	kilograms

1 Introduction and Goals

Maintenance of tidal inlets involves several problems and processes including scour, deposition, sand bypassing, navigation safety, and beach preservation. Hydrodynamics and sediment dynamics of tidal inlets are complex processes and not well understood. Advances in understanding the physical processes at inlets can be made by collection and analysis of field data, hydrodynamic numerical modeling, and analytical experiments designed to study flow and sediment transport patterns. One goal of the Coastal Inlets Research Program (CIRP) being conducted at the U.S. Army Engineer Waterways Experiment Station, Coastal and Hydraulics Laboratory (CHL) is to provide a unified and consistent understanding of hydrodynamic processes that control circulation and sand transport at tidal inlets. Results of studies conducted under CIRP will be incorporated by the U.S. Army Corps of Engineers (USACE) in design and maintenance procedures for navigation channels and associated structures, minimization of dredging requirements, and optimization of dredged-material placement for nourishment of downdrift beaches.

Another goal of the CIRP is the application and improvement of numerical modeling techniques for inlet and nearshore hydrodynamics. Recent advances in numerical modeling methods and computer technology have made it possible to conduct long-term simulations of inlet systems. Numerical primitive-equation models have been applied to navigation, dredging, and water quality problems, but have not yet been widely applied for engineering applications at tidal inlets. Physical process data collected at tidal inlets are required for verifying models and investigating hydrodynamics and sediment transport with high spatial and temporal resolution.

To assist the CHL in accomplishing these goals, under CIRP guidance the Florida Institute of Technology (FIT) conducted field-data collection during a 2-month-long field campaign at Ponce de Leon (Ponce) Inlet, located on the east coast of Florida (Figure 1). The field project was conducted between 21 August and 2 November 1997. Specific goals of CIRP addressed by this project include (a) quantifying hydrodynamic processes that relate to engineering activities at tidal inlets, (b) providing data for testing and validating numerical models of tidal inlets, (c) improving knowledge of structure-tidal flow interaction, and (d) improving knowledge of sediment transport at tidal inlets.

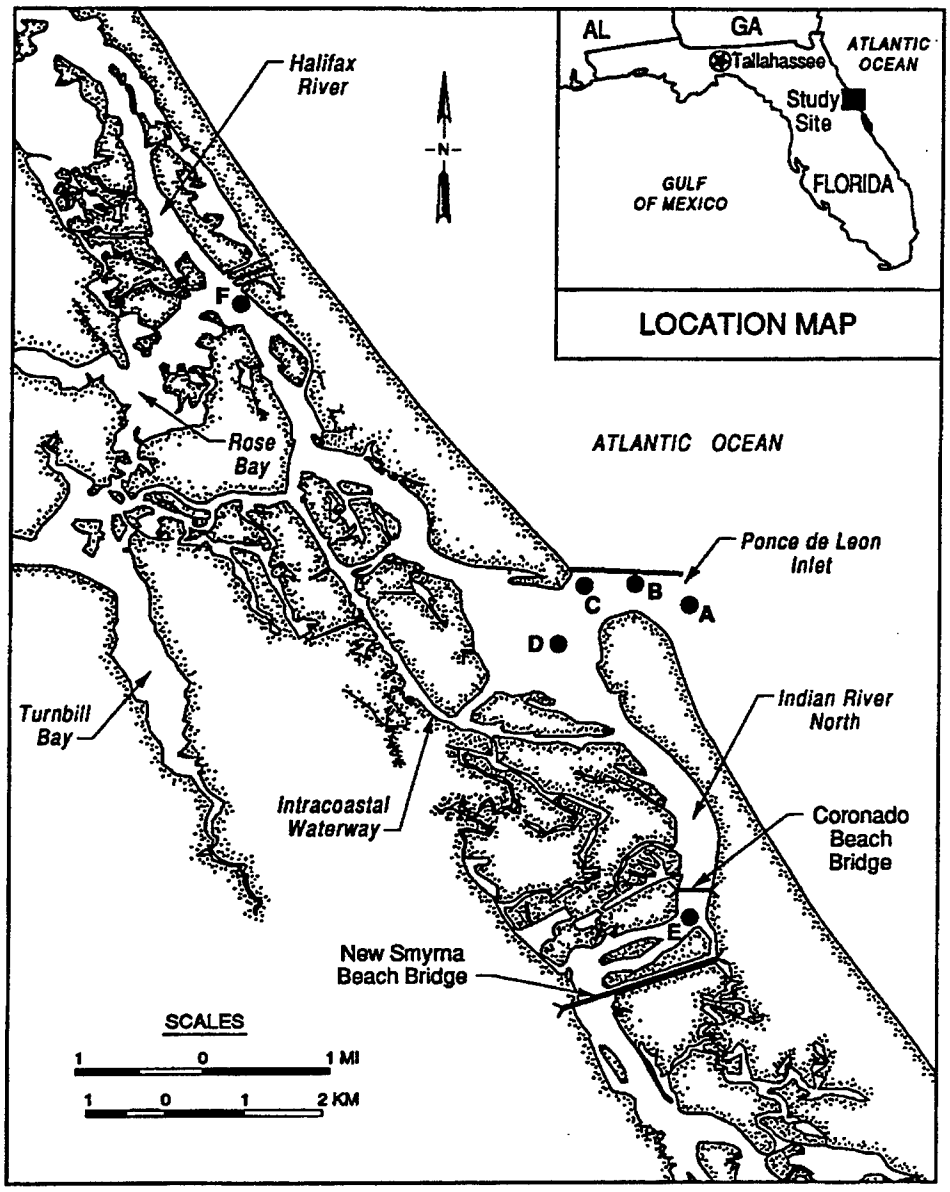

Figure 1. Ponce Inlet study area and location of monitoring stations

Project objectives for the field-data collection and analysis effort conducted in this study are as follows:

a. To provide a set of high-quality measurements of physical processes at a tidal inlet.

b. To analyze field data for spectral content of long and short (wind) waves at a tidal inlet.

c. To summarize field data in a convenient graphic format to illustrate properties of physical processes in the vicinity of tidal inlets.

d. To create a permanent archive of data collected during the project.

In addition, the field-data collection described herein augments long-term measurements at the site conducted under the CIRP (King et al. 1999).

This report is divided into four chapters. Chapter 1 is the Introduction and defines the goals and objectives of the subject study. Chapter 2 reviews the state of knowledge of physical processes at tidal inlets and provides a study site description. Chapter 3 discusses the study tasks and methods applied. Chapter 4 presents and discusses results of the study. Appendix A contains tidal constituents calculated from water-level measurements made during the data-collection effort. Appendix B contains a table for converting between calendar day and Julian day.

2 Overview of Inlet Processes and Study Site

Inlet processes related to inlet management and engineering are briefly described herein to provide background for interpretation of the data described in Chapter 4. A description of the Ponce Inlet study site is also provided.

Inlet Processes

Hydrodynamic processes in the vicinity of tidal inlets operate over a wide range of frequencies from small-scale turbulence in the benthic boundary layer to transient and seasonal changes in water elevation and circulation. In the direct vicinity of tidal inlets, water motion at diurnal and semidiurnal tidal frequencies dominates. Depending on nearshore and inlet morphology, the spectral composition of the tides can be significantly modified as the tide propagates through the inlet. Superimposed on transient and tidal processes are wind waves ranging in period from a few seconds to 15 sec or more. Similar to tidal motion, the spectral composition of waves can be modified by shoaling and breaking over variable shoreface and inlet topography. Moreover, interaction of wind waves with strong ebb and flood currents alters the physical properties of the waves.

Dynamic interaction of inlet hydrodynamics and morphology can also occur as a result of sand transport and associated topographic change. Processes and interactions must be better understood and be predictable to improve engineering and management practices at tidal inlets. Tidal inlet processes applied to coastal engineering studies are summarized in a series of technical reports by the USACE Coastal Engineering Research Center produced in the 1970s. Pertinent physical oceanographic aspects of tidal inlets and related environments are summarized in special publications (Aubrey and Weishar 1988; Aubrey and Giese 1992; van de Kreeke 1986). Studies of sand transport and morphologic change at tidal inlets and along the adjacent beach and shoreface can be found largely in the geoscience literature (Hayes 1979; FitzGerald 1984; Zarillo, Ward, and Hayes 1985; Zarillo and Liu 1990). These works are built on a foundation of basic studies of tidal inlet phenomenon that described the essentials of hydrodynamics and kinematics at inlets (Brown 1928; Keulegan 1951; Ozoy 1977; King 1974).

This body of previous work presents a consistent view of inlet hydrodynamics. The balance of forces at tidal inlets is predominantly between the pressure gradient and frictional forces. Gross sediment transport within the immediate vicinity of tidal inlet channels can be directly related to these forces.

However, the detailed patterns of sediment transport and net transport entering engineering applications can only be understood by considering some of the nonlinear aspects of tidal motion and wave-current interaction. Energy in long (tidal) waves approaching an inlet undergoes reflection, dissipation, and transmission. During transmission the spectral components of the tidal wave can change depending on the local coastal geomorphology and composition of the ocean tide. Nonlinearities generated in the tidal wave as the spectral composition of energy changes in the tidal wave are termed overtides. The frequencies of energy in overtides can be determined by application of harmonic and spectral methods to analyze tide measurements (water level and currents). A second source of tidal asymmetry is the long-term pressure gradients between the ocean and bay. These pressure gradients will enhance ebb or flood flow through the inlet, depending on the direction of tilt of the water surface. Tidal asymmetry in shallow water in part controls the net transport direction of near-bed sand transport in the major inlet channels, thus having a significant impact on the trapping and impounding of sediment in inlet shoals.

Observations of sedimentary structures, bed phase morphology, and migration of large-scale sand bodies on tidal shoals indicate the presence of the wave-current interaction in driving sand transport in these areas. Qualitative observations have confirmed the significance of sand exchanges between inlet shoals and adjacent barrier island systems as controlling sediment budget and sand bypassing (FitzGerald 1984; Zarillo, Ward, and Hayes 1985). Thus, many problems in coastal engineering near tidal inlets can be related to wave- and tidal-current driven sand movement.

Site Description

Ponce Inlet is located on the east coast of Florida and lies approximately 92 km (57 miles) north of Canaveral Harbor (Figure 1). Historically, Ponce Inlet has been difficult to navigate because of channel migration, shallow water adjacent to the channel, and strong wave-current interaction (Harkens, Puckette, and Dorrell 1997). The inlet became a Federal navigation project in 1968 when stabilization by jetty construction was initiated. Jetty construction was completed in 1971. Two jetties were constructed and a weir section was built into the north jetty to function in a sand bypassing capacity. The weir did not function as anticipated, and scour occurred in the northern inlet throat while the south spit migrated into the inlet (Parthenaides and Purpura 1972; Purpura 1977; Jones and Mehta 1978). The weir was closed in 1984, but scour at the north jetty and encroachment of the south spit into the inlet has continued (Taylor et al. 1996; Harkins, Puckette, and Dorrell 1997). Upon weir closure, the north interior spit, located west of the north jetty, has eroded (Harkins, Puckette, and Dorrell 1997). Presently, the south jetty is almost entirely buried by sand.

Ponce Inlet connects northward to the Halifax River and southward to the Mosquito Lagoon via the Indian River North (Figure 1). The mean tidal range in the ocean is approximately 1 m (3.3 ft), and the mean spring range reaches 1.3 m (4 ft). The tide is semidiurnal with the M_2 amplitude dominating other constituents by an order of magnitude. A navigation channel was dredged west of the bay in the 1950s as part of the Intracoastal Waterway (IWW) system (Figure 1). The IWW traverses the length of the study site and is the major

channel within the Halifax River/Mosquito Lagoon complex away from the inlet. Design dimensions of the IWW are 90 m (300 ft) width and 3.7 m (12 ft) depth. The confluence of the IWW and the Halifax River lies 3.5 km north of the inlet, and the IWW joins the Indian River North 2 km south of the inlet.

West of the inlet, the flood shoal occupies a significant amount of the bay area. The flood shoal is exposed during much of the tidal cycle so that flow is commonly restricted to the main channel and Rockhouse Creek, a tidal channel that bifurcates the flood shoal. Other natural features in the area include Rose Bay and Turnbill Bay and numerous small channels that provide water exchange for marsh and mangrove habitats of the area. These channels and bays act as storage for water flowing into and out of the Ponce Inlet system. The Coronado Beach Bridge crosses the Indian River North approximately 4 km south of Ponce Inlet.

3 Project Tasks and Methods

The field data-collection campaign consisted of planning, preparation, and deployment of six instrumented moorings, data retrieval, and data analysis. Details of these study components are discussed in this chapter.

Logistics and Marine Operations

The project described herein began on 1 July 1997. The initial tasks included planning of logistics, configuration and calibration of instrument packages, and construction of mooring systems for six monitoring stations. Construction of moorings and sensor packages was completed in approximately 5 weeks. Two large moorings for puv-type wave gauges at Stations B and C (Figure 1) were deployed on 9-10 August 1997. The 800-lb[1] wave-gauge moorings consisted of modified railroad wheels and were deployed from FIT's 65-ft research vessel R/V *Delphinus*.

Sensor packages were deployed for all six stations on 21-22 August 1997. Station A was deployed on a 12-ft stainless steel pylon jetted approximately 2.5 m into the sand on the ebb shoal (Figure 1). The interior (located landward of the inlet) sensor packages at Stations D through F were deployed on aluminum quadripods fixed to the sediment bed by cement blocks and spiral anchors. These interior stations were leveled with respect to the National Geodetic Vertical Datum (NGVD) by rod and transit surveys from nearby National Ocean Service (NOS) benchmarks. Wave gauges at Stations B and C were fixed to the railroad wheel moorings deployed on 9 August 1997. Field log sheets describing the time, location, and activities during deployment and retrieval of the monitoring systems were maintained and used to guide postprocessing of data.

Measurement of Waves, Currents, and Water Level

Measurements of directional waves, current velocity, and water level were obtained at six locations in the Ponce Inlet system (Figure 1). The overall measurement strategy was aimed at collecting data for model calibration, calculating the spectral distribution of tidal and wind-wave energy, and examining the processes involved in spectral filtering of the tide as it propagates from the coastal ocean into the back-bay system. Measurement locations, shown in Figure 1, were selected to capture processes occurring on the ebb shoal, in the

[1] A table of conversion factors from non SI to SI units of measurement is given on page vii.

inlet, and in the bay channels away from the inlet. Station A was located on the ebb shoal approximately 2.5 km from the outer inlet throat. Stations B and C were located within the inlet throat. Station D was deployed in the back bay, in an area of direct influence of the inlet. Stations E and F were located south and north of the inlet, respectively, and positioned upstream of the confluences of the IWW and the natural tidal channel (Figure 1).

Stations D, E, and F were deployed in the back-bay portion of the project area. These stations were designed to collect current velocity and water-level data (no short waves). Station D was located near the confluence of the inlet conveyance channel and the natural tidal channel system. These two stations were leveled with respect to NGVD. The temporal sampling scheme for the stations was designed to capture semidiurnal tidal and lower frequencies of motion. Wave data were collected in 20-min bursts of 2048 data points sampled at 1 Hz. Current velocity and pressure data were collected at a sampling rate of 1 Hz. Hourly current velocity and water-level values were calculated from 1-min averages of 1-Hz samples.

Data at the six fixed stations were collected over a 75-day interval beginning on 21 August 1997 and ending on 1 November 1997. All sensors were calibrated before and after field deployment. The electromagnetic current sensors were factory calibrated by Marsh-McBirney, whereas the pressure sensors were calibrated by FIT.

The primary system for fixed-station monitoring consisted of a two-axis electromagnetic sensor combined with a high-resolution pressure transducer (puv-type sensors). System configuration is shown in Figure 2. Components of the combined current and directional wave sensor include an embedded data logger/controller with additional data storage memory, an electromagnetic two-axis current velocity sensor, a high-accuracy stable pressure transducer, a digital fluxgate compass, and battery pack.

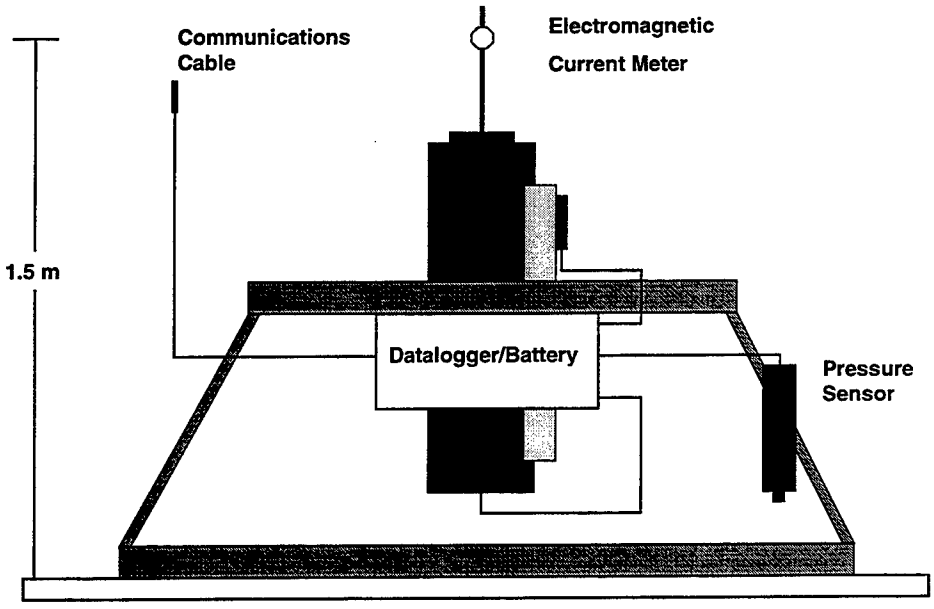

Figure 2. Schematic view of sensor package

Data Analysis Methods

Calibration records were maintained for all sensors and applied to quality check the data acquired during the 10-week field campaign. Raw data from the field deployment were converted to engineering units by applying calibration data maintained for each sensor. Prior to finalizing data conversion, all sensors were recalibrated and calibration statistics compared with predeployment statistics. In all cases, postfield calibration remained well within sensor resolution. Once the calibration process was completed, water-level data for Stations D, E, and F were related to datum (NGVD) based on leveling surveys to nearby benchmarks. Stations A, B, and C were too distant from benchmarks and too deep to allow accurate leveling surveys. Therefore, water-level data were referenced to the mean water elevation of the records at these inlet and ebb-shoal stations.

Comparisons of current speed, current direction, and water-level time series were made among the six stations to determine if water level, tidal phase, tidal amplitude, and current magnitude were consistent with respect to station position and inlet geometry. This review resulted in the elimination of short segments of Station A and Station E data that may have been contaminated by low battery power or electronic noise.

NOS standard harmonic analysis methods were applied to all water-level data from stations having continuous records of 29 days or longer to calculate tidal constituents. Where possible, harmonic analysis of overlapping 29-day segments of water-level data were conducted, and the results were vector averaged to provide a more stable estimate of tidal constituents. Shortened time series at Stations A and F allowed harmonic analysis on a single 29-day record in each case.

Wave data were processed by spectral analysis to extract the frequency and directional spectra for each wave burst. Data were averaged over three bands at a band width of 0.01 Hz, and the analysis was performed with 16 degrees of freedom. Wave-data analysis was performed by application of a low-frequency cutoff of 20 sec (0.05 Hz) and a high-frequency cutoff of 3 sec (0.33 Hz) to prevent aliasing and folding of energy into lower frequencies. All time stamps attached to the analysis were in terms of Eastern Standard Time (EST).

Data Archiving

FIT maintains a permanent record of the data collected during field operations in a format convenient for both time-series analysis and comparison with numerical model calculations. Data collected during the field data-collection campaign are stored on several media to ensure permanent and convenient retrieval. Raw data sets returned from the field were placed on backup tape and disk. Duplicate backup tapes containing all data were created along with copies of data stored permanently on hard disk space assigned to the project. FIT will maintain data for a minimum of 10 years.

Similarly, postprocessed data sets are stored on both backup tape and hard disk media in several locations within the FIT computing network. The results of

time-series analysis of postprocessed data were provided to CHL in electronic form for graphical presentation and further analysis.

4 Site Investigation Results

Water level, current, and wave data collected at the six measurement stations at Ponce Inlet and in the interior bay channels are presented and discussed. Wave parameters and water level are provided in forms of time series and spectra.

Data Return

Performance of the six monitoring stations is given in Table 1 according to parameters, location, and data return. The overall data return is 75 percent with respect to the original monitoring plan. When damage to the two inner wave gauges is accounted for, the data return rises to approximately 85 percent.

Table 1
Monitoring Station Performance

Station	Location	Deployment Duration	Parameters	Data Return, percent
A	Ebb shoal	8/22 – 11/1/98	Waves, water level, current	76
B	Inlet channel	8/22 – 10/2/98	Waves, water level, current	100
C	Inlet channel	8/22 – 10/2/98	Waves, water level, current	100
D	Conveyance channel	8/22 – 11/1/98	Water level, current	100
E	Back bay – south	8/22 – 11/1/98	Water level, current	95
F	Back Bay – north	8/22 – 11/1/98	Water level, current	50

Wave Statistics and Spectra

Wave statistics and spectra are reported in this section for Stations A, B, and C. There are limitations to the analysis because the puv-type wave gauge deployed for this project cannot adequately resolve directional wave energy for conditions that are not nearly monochromatic. Therefore, it is possible that considerable wave energy arrived from other directions and was not included within the directional spectrum.

Significant wave height and wave period at Station A are shown in Figure 3. The time axis on this and other time-series plots is shown in Julian days (JD). A table for conversion between calendar day and Julian day is given in Appendix B. Significant wave heights ranged from approximately 0.4 to 1.7 m. The average

significant wave height was 0.7 m, and the most frequently occurring, or modal, wave height was 1 m. Wave periods were reported from the spectral bin containing the greatest energy and spanned the range from 4 to 13 sec. The average wave period among the recorded bursts was approximately 9 sec. Wave periods above 10 sec were common at Station A. Here, the modal wave period was 12 sec. Significant wave height and direction are shown in Figure 4 for Station A. During the measurement interval, energy approached Ponce Inlet from the northeast (60 deg).

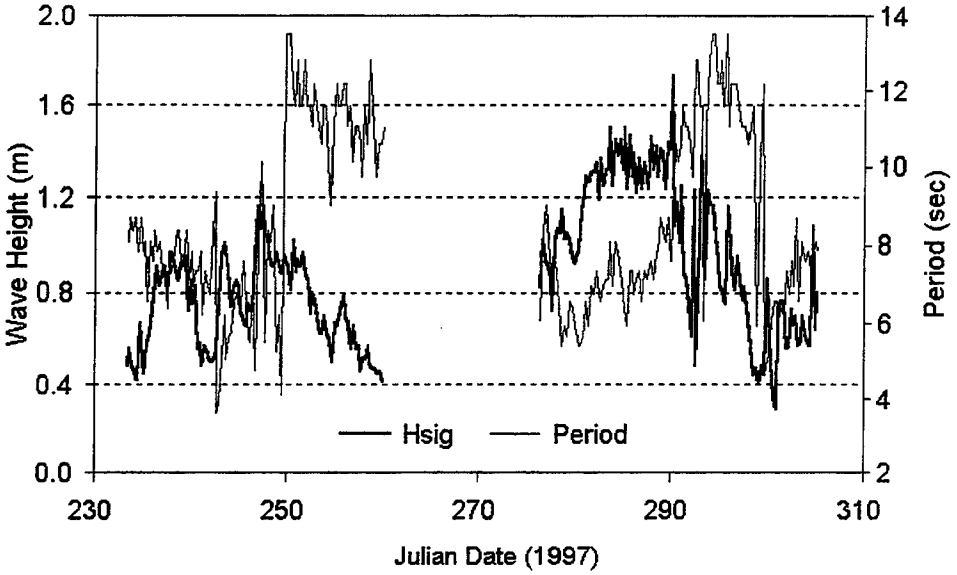

Figure 3. Significant wave height and peak period at Station A

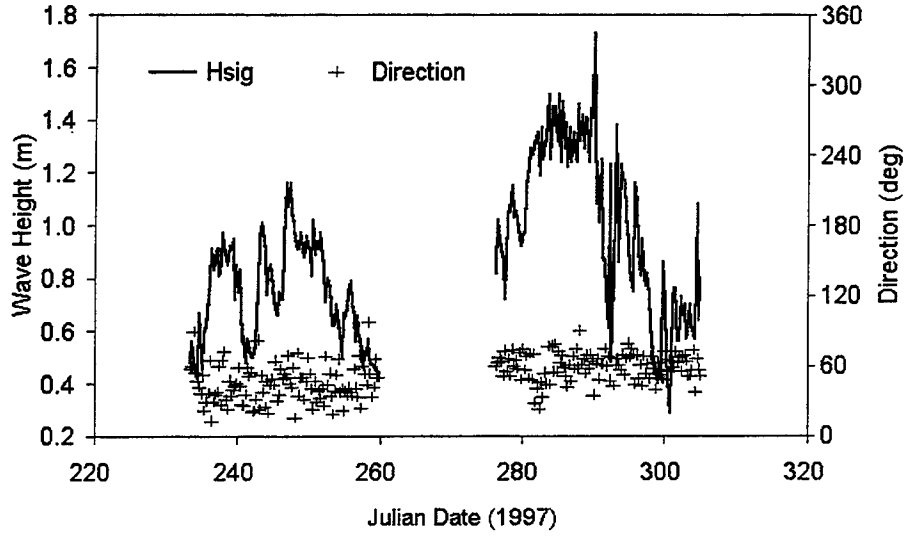

Figure 4. Significant wave height and peak direction at Station A

Significant wave height and period at Station B are shown in Figure 5. Significant wave heights are typically less than 1 m, with the average significant

wave height being 0.62 m. However, wave records at Station B occasionally show significant wave heights that exceed 1.5 m and have maximum values of 2 m. These relatively large wave heights occurred almost exclusively as occasional individual bursts and were at relatively long periods (8 to 12 sec). Significant wave height and period at Station C, shown in Figure 6, are similar to those at Station B, including the occasional 2-m waves. However, typical significant wave height at Station C is below 1 m. A comparison of significant wave heights at the three inlet stations, plotted in Figure 7, shows that Station A is more energetic as compared with the inlet throat stations with the exception of large peaks at Stations B and C. The lower energy experienced at Stations B and C is a result of filtering of waves by the inlet. Wave direction at Stations B and C is not shown because the inlet constrains direction.

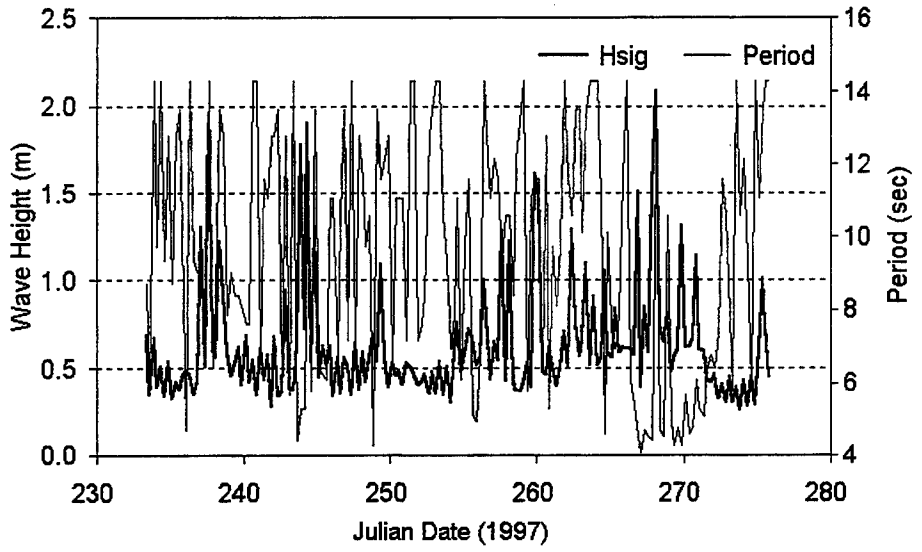

Figure 5. Significant wave height and peak period at Station B

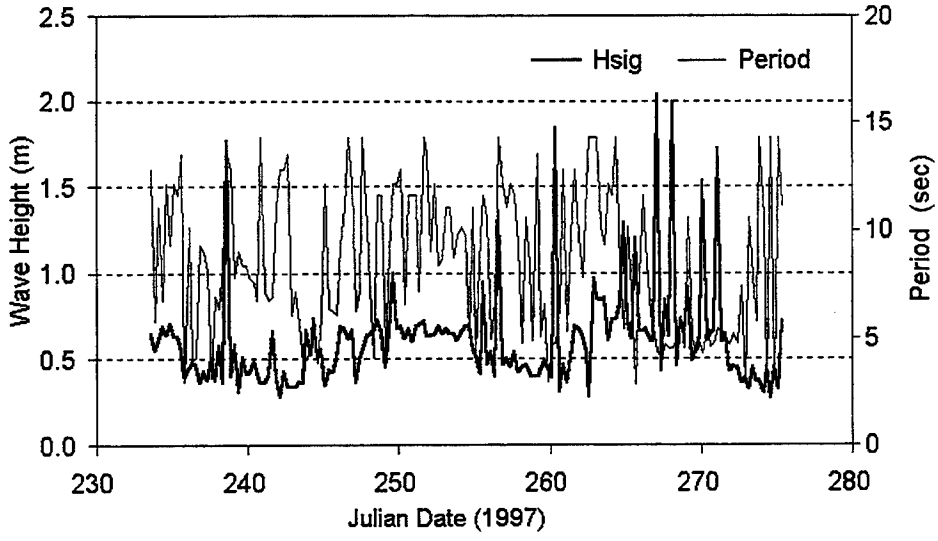

Figure 6. Significant wave height and peak period at Station C

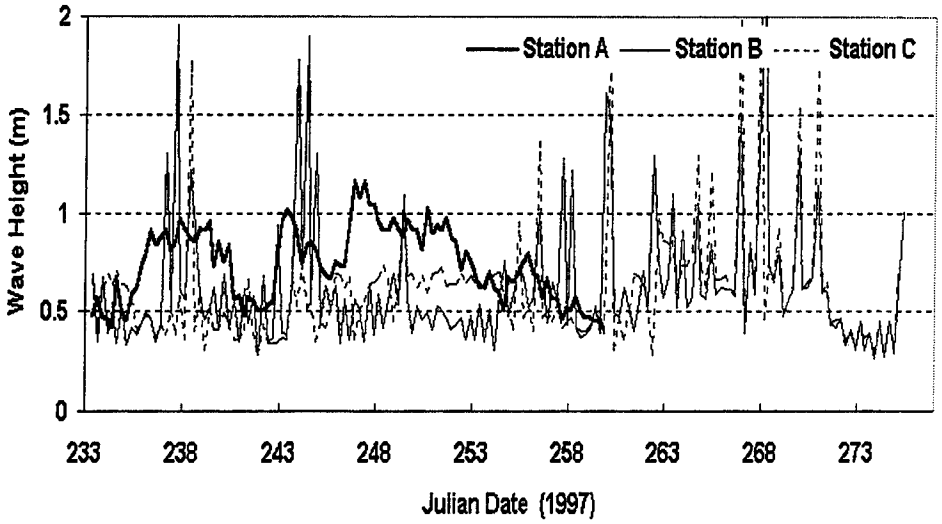

Figure 7. Significant wave height at Stations A, B, and C

Spectra at Stations A, B, and C are compared in Figure 8 for a time when the wave energy at Station A was relatively high (2130 hours on 4 September 1997 (JD 247.8958)). The spectrum at Station A is broad banded with relatively high peak-wave energy at about 8 sec (0.125 Hz). Secondary energy peaks occurred at periods between 6 sec (0.17 Hz) and 3 sec (0.33 Hz). The corresponding spectra at Stations B and C show some energy between 6 and 13 sec (0.08 Hz), but it is significantly lower than at Station A. Energy at higher frequencies is not present or resolved at Stations B and C.

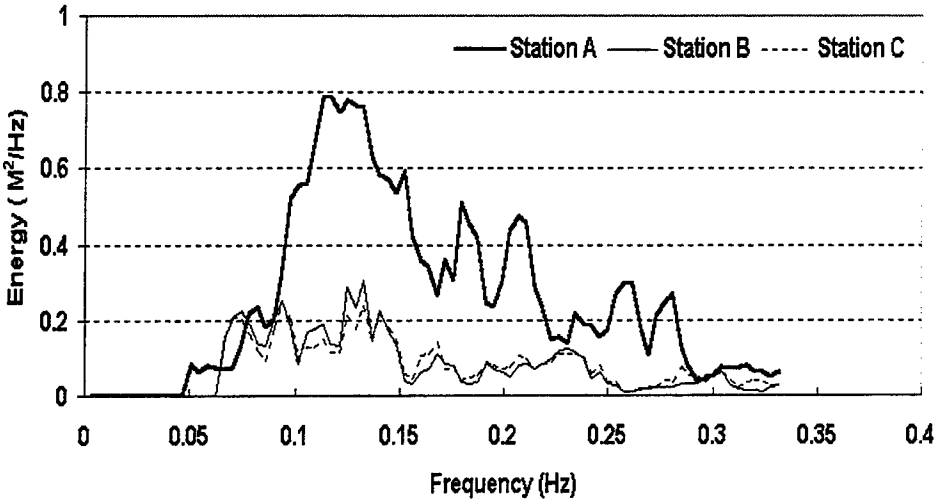

Figure 8. Spectra of wave height for Stations A, B, and C at 2130 on 4 September 1997

Figure 9 compares spectra from the inlet during a time of relatively low-wave energy recorded at all stations. In this case, wave spectra from 2130 on 24 August 1997 (JD 236.8958) contained significant energy in fewer frequency bands as compared with that shown in Figure 8. Additionally, significant wave

heights calculated at all the stations were below 0.6 m. Higher energy conditions at a particular station usually correspond to broader banded spectra. Figure 10 shows wave spectra for high- and low-wave energy at Station A. Low-energy waves that occurred on 23 August 1997 (JD 235) had a narrower banded spectrum than those on 25 August (JD 237) and 4 September (JD 247) 1997 during which the wave energy was higher. Figure 11 compares spectra from Stations A, B, and C for 0330 on 13 September 1997 (JD 256.1458). Peak energy at 11.5 sec (about 0.09 Hz) is present in the spectrum of Station A, along with a secondary peak at approximately 6 sec (0.17 Hz). However, the spectra of Stations B and C include no distinctive energy peaks, and most of the energy is distributed over the higher frequency spectral bins. Data from which these spectra were computed were recorded at lower tide levels, and the higher energy seen in the spectrum of Station A may have been dissipated by wave breaking over the ebb shoal.

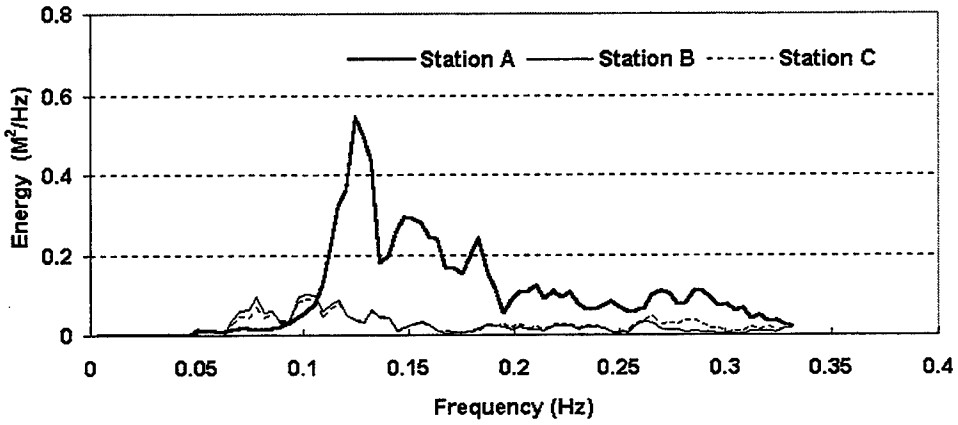

Figure 9. Spectra of wave height for Stations A, B, and C at 2130 on 24 August 1997

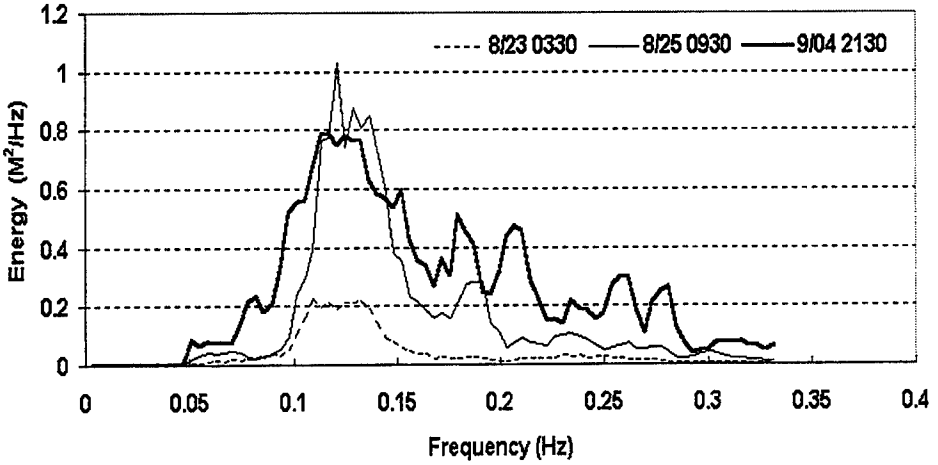

Figure 10. Comparison of lower and higher wave-energy spectra at Station A

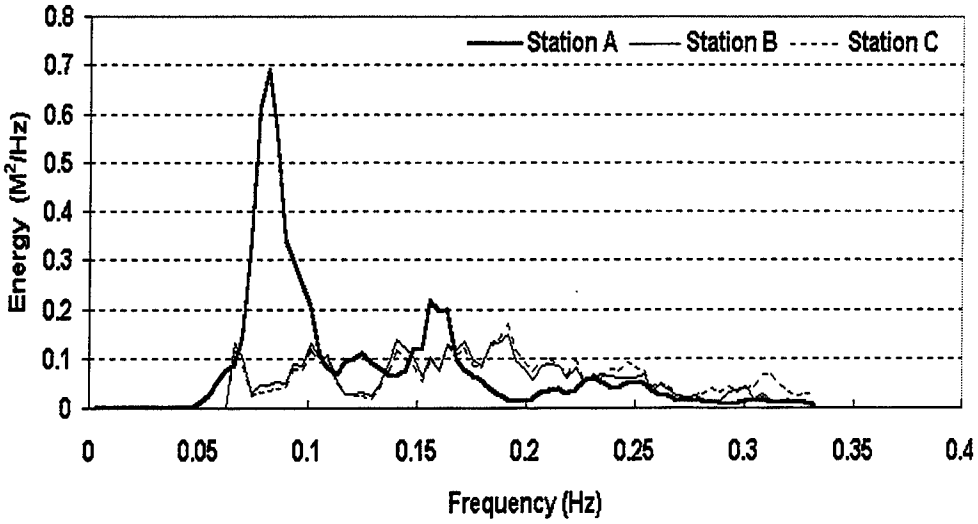

Figure 11. Comparison of lower wave-energy spectra at Stations A, B, and C at 0330 on 13 September 1997

Tidal and Subtidal Motion

Water level and current measured at the six monitoring stations are described in terms of their time series and spectral properties. Specifically, tidal and subtidal motions are described. In this discussion of water level and current, the term "subtidal" refers to motion that varies more slowly than the diurnal tidal motion and is of nontidal origin.

Water level at Station A is shown in Figure 12 where the water-level values were reduced to the time-series mean because the station was not leveled to the NGVD datum. The water-level record contains a range of as much as 1.8 m during spring tide, which decreases to less than 1.3 m at neap tide. A diurnal inequality in the tide is present in the water-level record. The record shows strong subtidal motion from the beginning of the time series to JD 260 (17 September), when the station's battery power dropped and record quality degraded. During the second month of deployment, the magnitude of subtidal motion was negligible.

The current record at Station A is shown in Figure 13. The current has a strong tidal signal, reversing direction at the M_2 frequency and occasionally reaching a maximum of more than 1 m/sec during spring tide. In Figure 13 and all other figures showing current direction, 0 deg indicates flow toward the north, and 90 deg indicates flow toward the east. Diurnal inequality in flood current and ebb currents is present and consistent with the water-level signal.

Figure 14 compares current speed and water level at Station A for a 3-day interval starting on JD 290 (17 October). Positive values of the current correspond to ebb flow, and negative values indicate flood flow. Peak flood current was consistently stronger than peak ebb current (shown in detail in Figure 14). Flood dominance was found at all monitoring stations over the measurement interval and is included in discussion of data from each gauge.

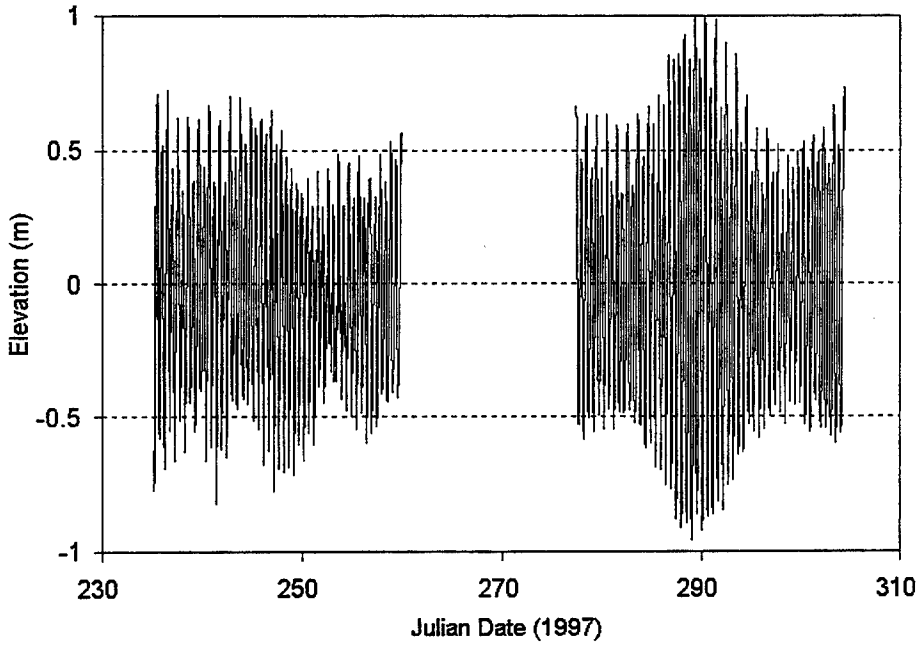

Figure 12. Time series of water level at Station A. (Data are reduced to time-series mean)

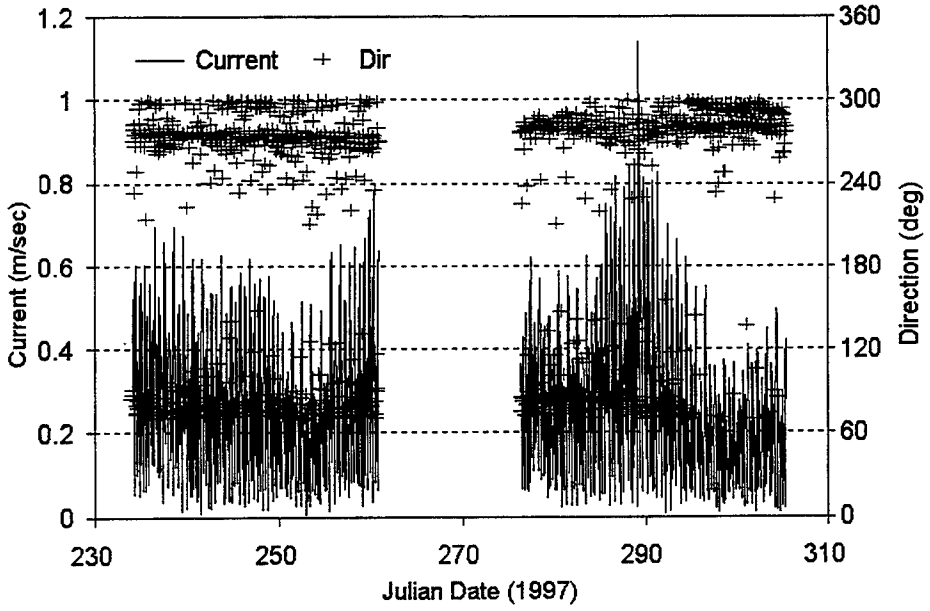

Figure 13. Time series of current speed and direction at Station A

The flood current may have been enhanced by a landward-directed subtidal flow so that its peak had consistently greater magnitudes than the ebb current peak. Maximum flood current magnitude can be 50 to 80 percent higher than the maximum ebb current magnitude.

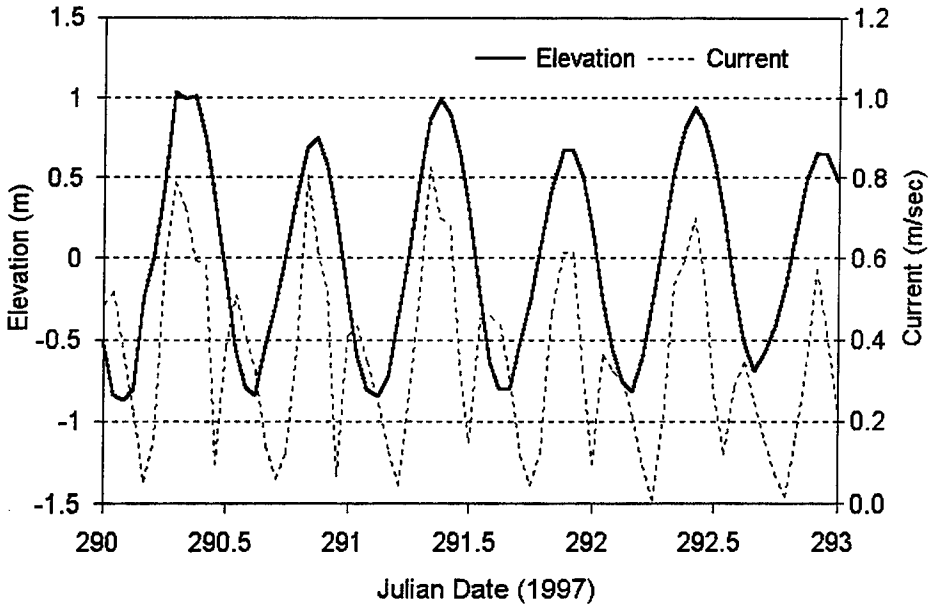

Figure 14. Time series of current and water level at Station A

Water level and current measured at Station B are plotted in Figures 15 and 16, respectively. The tide possesses a diurnal inequality, and the tidal range reaches a maximum of approximately 1.8 m. Similar to the current measured at Station A, maximum flood current magnitudes observed at Station B were as much as 80 percent higher than corresponding maximum ebb current. Landward-directed mean flow was also strong at this station and contributed to the flood dominance of the inlet.

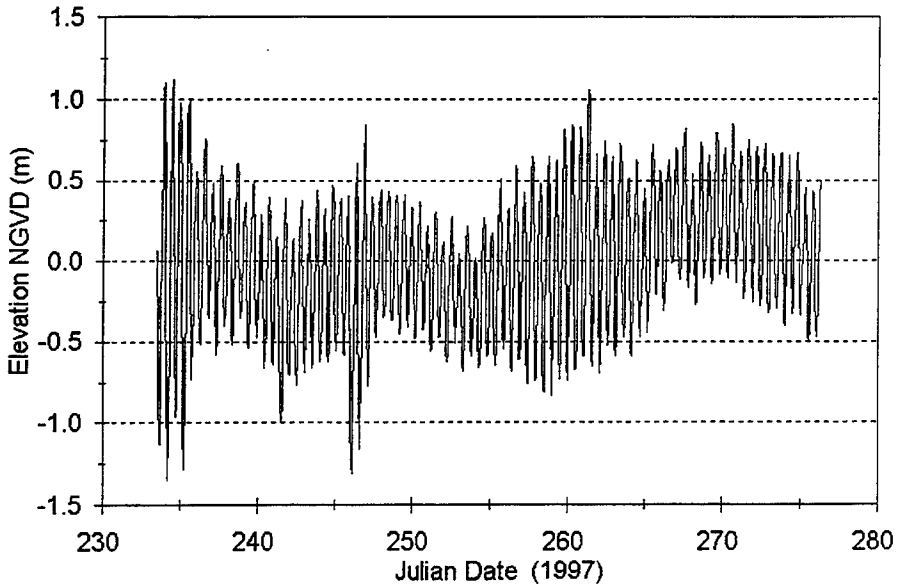

Figure 15. Time series of water level at Station B from 22 August to 1 October 1997

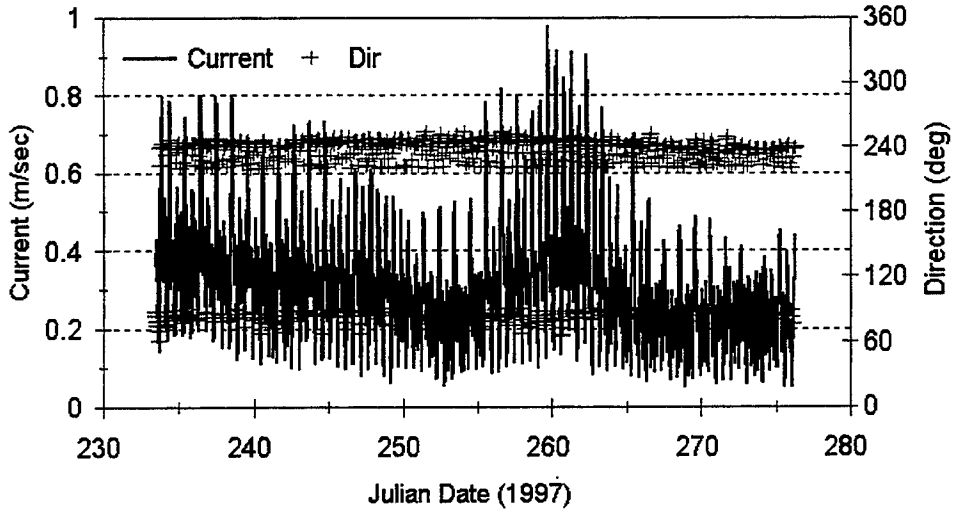

Figure 16. Time series of current speed and direction at Station B

Water level and current measured at Station C, shown in Figures 17 and 18, respectively, have similar patterns to those recorded at Station B. Maximum tidal range during spring tide reached 1.8 m and decreased to approximately 1.2 m at neap tide. Maximum tidal current speed ranged between approximately 0.4 m/sec and 1.4 m/sec. Subtidal flow at Station C resulted in the same pattern of flood-ebb current inequality observed at Stations A and B.

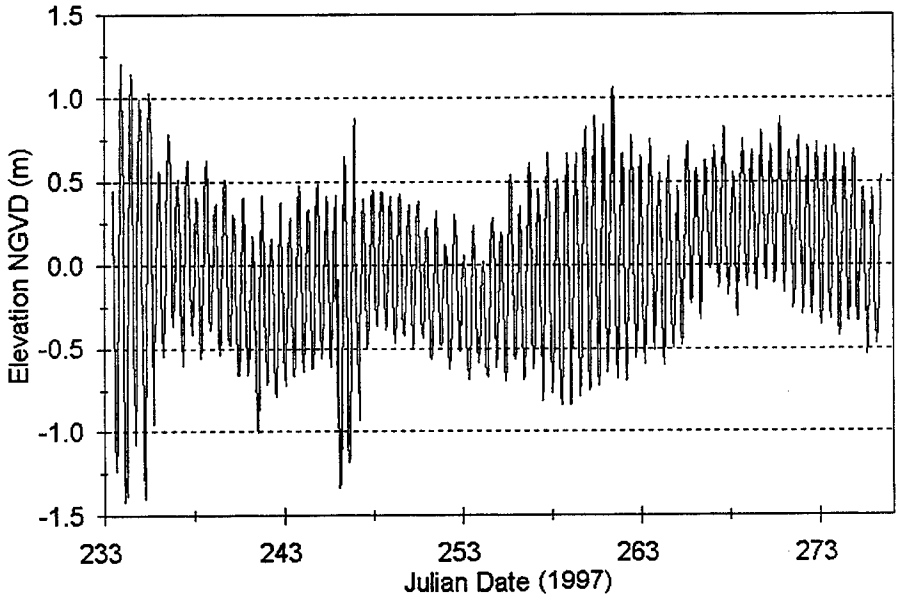

Figure 17. Time series of water level at Station C from 22 August to 1 October 1997

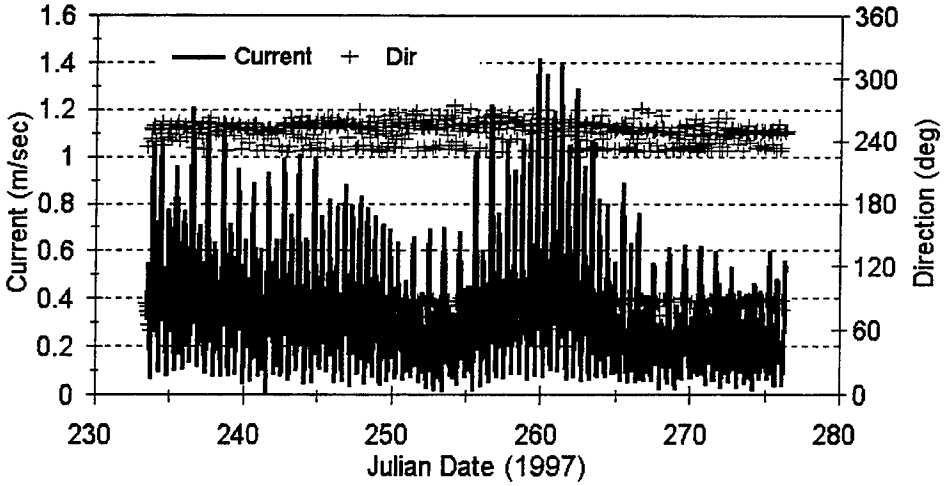

Figure 18. Time series of current speed and direction at Station C

Figure 19 compares water level at hourly intervals at Stations B and C over a 5-day interval starting on JD 234 (22 August). The tidal curves are offset in time between the two stations. Harmonic analysis gives a 14-deg difference in phase between the semidiurnal water-level curves at Stations B and C. This phase difference represents the time lag of approximately half an hour between stations as the tidal wave propagates through Ponce Inlet.

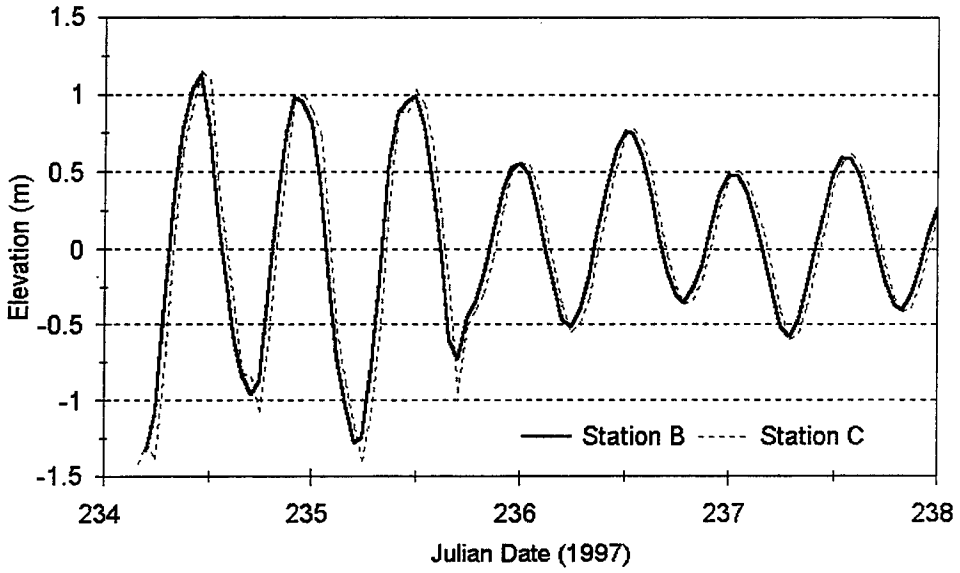

Figure 19. Time series of water level at Stations B and C

Figures 20 and 21 show the record of water level and current velocity, respectively, at Station D. The tidal range at Station D varies from approximately 1.6 m at spring tide to 0.6 m during neap tide. The semidiurnal tide possesses a diurnal inequality. Tidal currents recorded at Station D are similar in magnitude to those recorded at Stations B and C. Maximum flood

currents commonly exceed 1 m/sec during spring tide. Similar to data recorded at other stations, maximum flood current magnitudes are much larger than maximum ebb current magnitudes. This inequality is in part controlled by the strong subtidal flow, which varied from 0.2 m/sec to greater than 0.5 m/sec at Station D during monitoring.

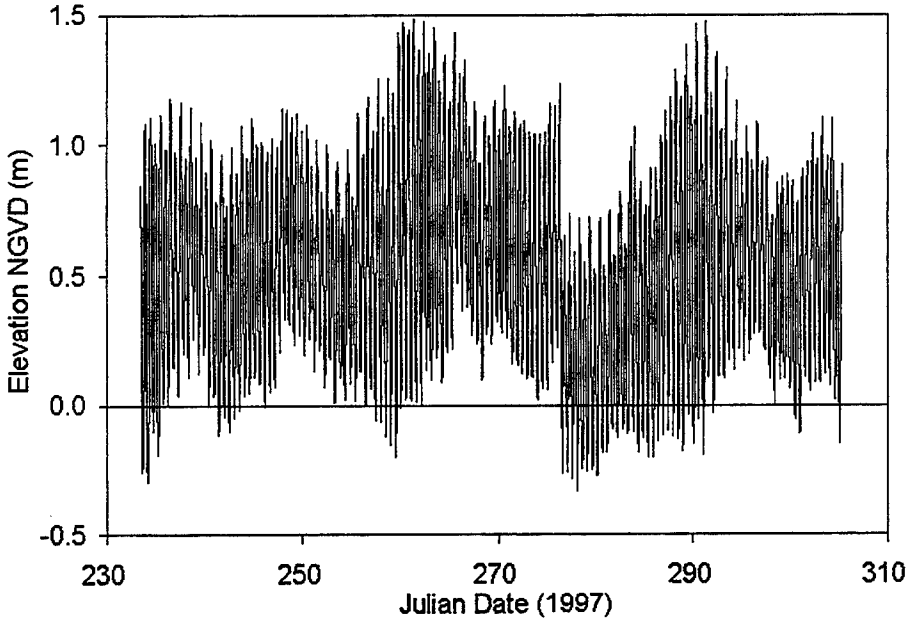

Figure 20. Time series of water elevation at Station D

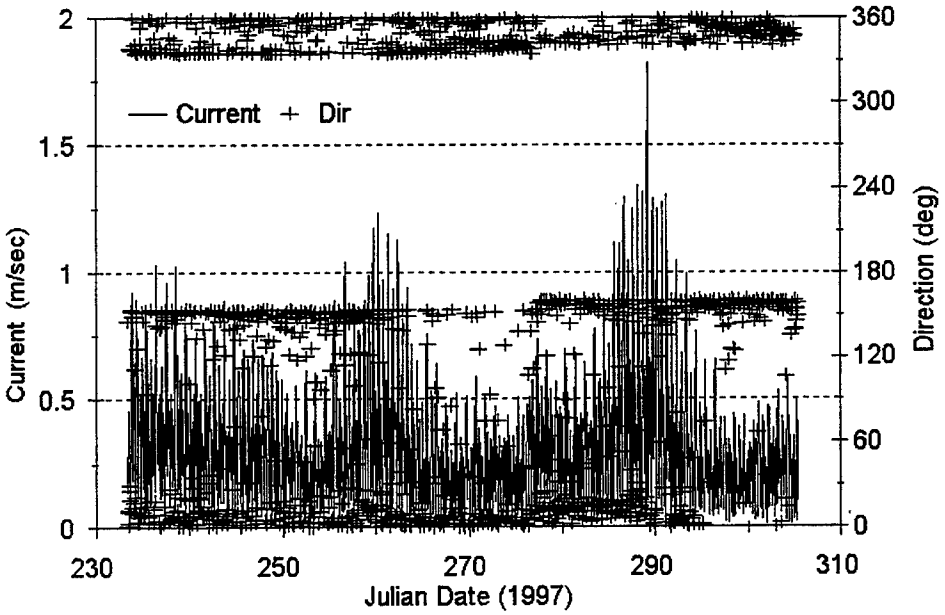

Figure 21. Time series of current speed and direction at Station D

Water level measured at Station E is shown in Figure 22. The gap between JD 268 (25 September) and JD 272 (29 September) at Station E is related to electronic noise caused by a power cable leak. This problem was repaired, and all other sections of the elevation record can be considered reliable. The maximum observed tidal range was approximately 1.5 m during a spring tide on JD 260 (17 September). At neap tide the range decreased to approximately 0.5 m.

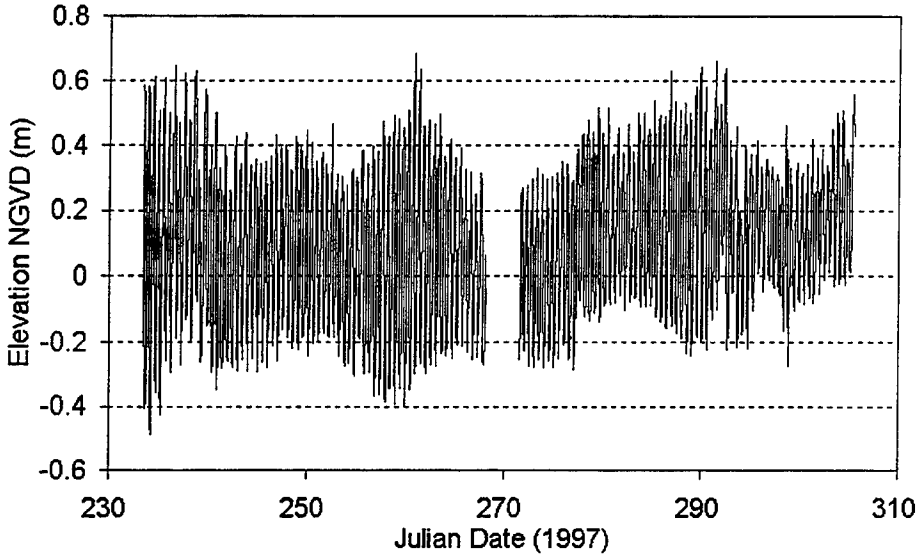

Figure 22. Time series of water level at Station E

Current speed and direction at Station E are shown in Figure 23. The current was directed toward the south-southwest during most of the measurement interval. Current magnitudes fluctuated at the diurnal tidal frequency, but rarely reversed direction. Current speeds recorded at Station E were weaker than those measured at stations located closer to Ponce Inlet and were less than 0.5 m/sec during most of the data-collection effort. Two periods of particularly strong subtidal flows occurred during monitoring, one centered at JD 270 (17 September) and the other beginning on JD 291 (18 October) just after spring tide and extending to JD 298 (25 October) (Figure 23). The second event is also captured in the current measured at Station D. The sources of these strong events were not investigated.

Water level at Station F is shown in Figure 24 for the time interval JD 274 (1 October) through JD 305 (1 November). Data collected at this station prior to 1 October were contaminated by water from a leaking bulkhead connector. During October an increase in the mean elevation of approximately 0.4 m was superimposed on the tidal signal. A maximum tidal range of approximately 1 m was observed at spring tide, whereas the neap tide range was approximately 0.5 m.

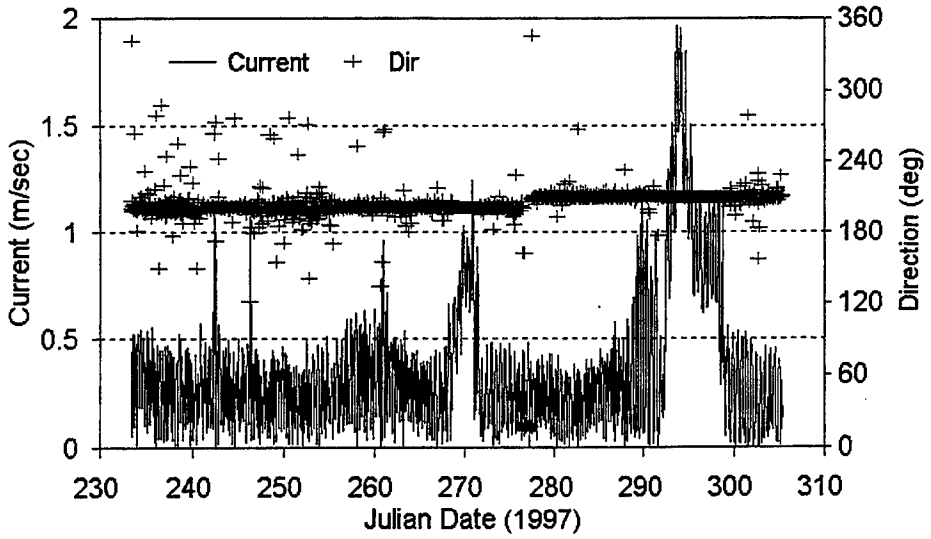

Figure 23. Time series of current speed and direction at Station E

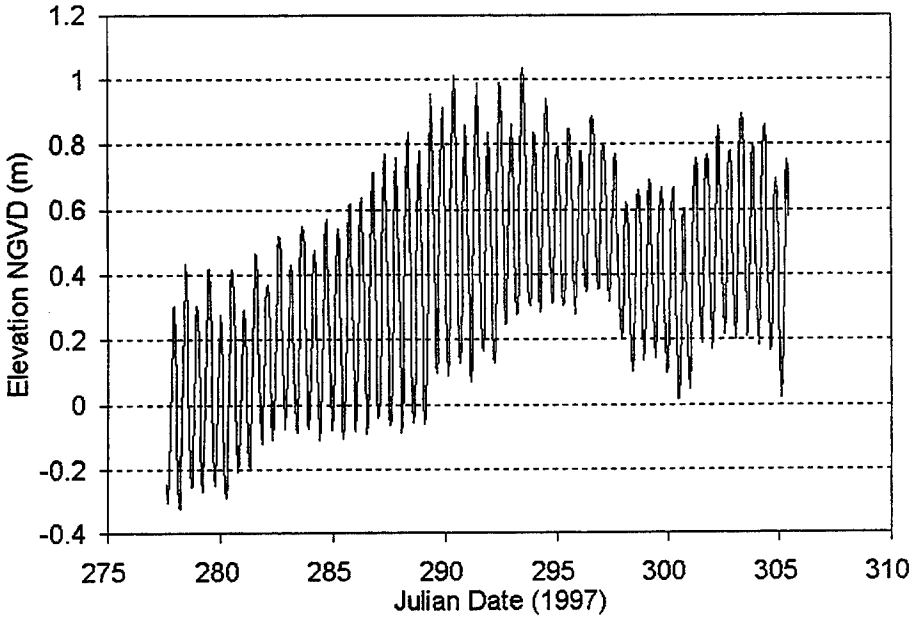

Figure 24. Time series of water level at Station F

Currents observed at Station F, shown in Figure 25, were the weakest of the six stations. Tidal currents were superimposed on a strong subtidal current flow and displayed the same flood-ebb inequality observed at all other stations. Magnitude of the subtidal flow was reduced during the latter half of the time series. During some segments of the data, tidal currents were not strong enough to reverse the subtidal flow direction. For instance, from JD 301 (28 October) to the end of the series, the current speed oscillated at the tidal frequency; but flows remained direct to the north-northeast.

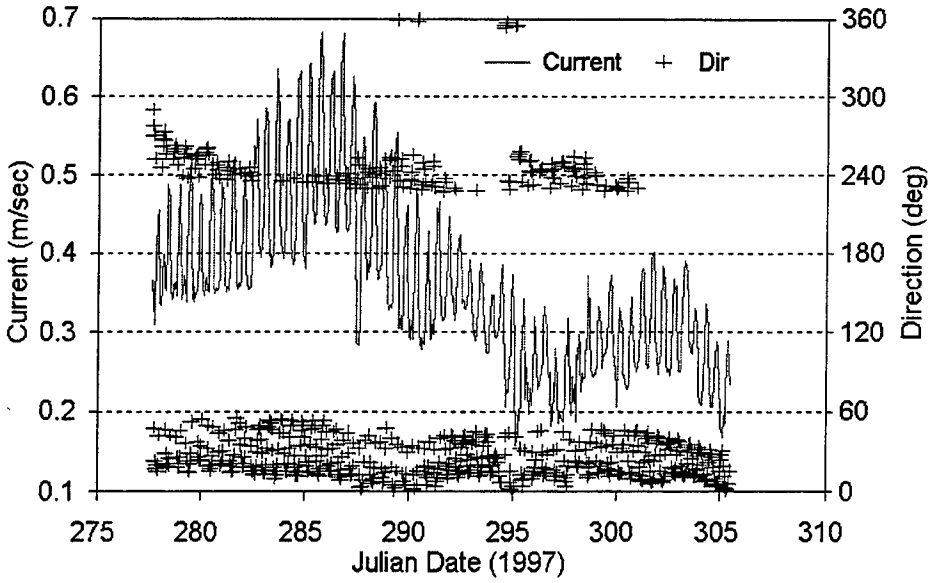

Figure 25. Time series of current speed and direction at Station F

Figure 26 compares tidal elevation among Stations D, E, and F for the 5-day period between JD 285 (12 October) and JD 290 (17 October). The tidal range is reduced at Stations E and F as compared with Station D, illustrating attenuation of the tidal signal as it propagates through the interior bay channels. The tide range at Station E is persistently smaller compared with the other back-bay stations. It is noteworthy that Station E is located 1 km south of Coronado Beach Bridge. The bridge restricts channel dimensions, dissipates energy, and limits exchange. The bridge increases attenuation of tidal energy and influences water levels beyond what can be expected for the natural channel dimensions in this area (Militello and Zarillo 1999).

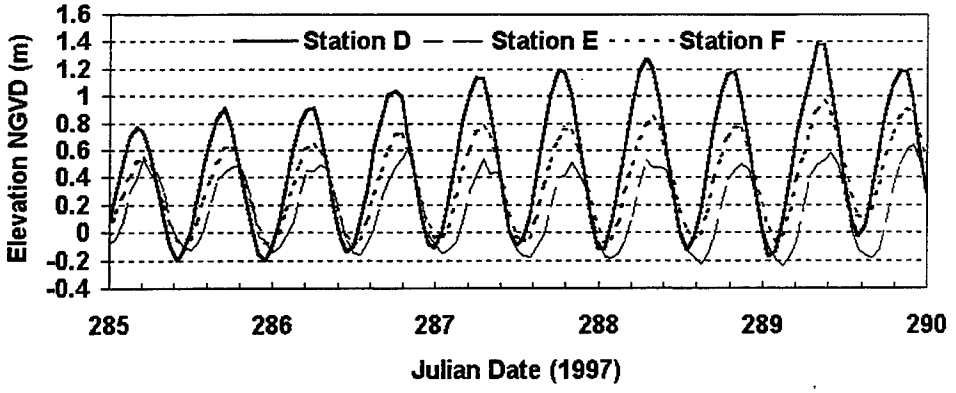

Figure 26. Tidal elevations at Stations D, E, and F from 12 October to 17 October 1997

Figure 27 compares the tidally averaged water elevation at Stations A and D for the period of JD 279 (6 October) through JD 304 (31 October). De-meaned water-level signals were plotted because Station A was not leveled to NGVD. To make the comparison, it was assumed that the mean water elevation at Station A

remained at or above the mean elevation of Station D throughout the monitoring interval. This assumption is justified by consideration of the mean flow of water that was directed into the inlet at all times, which indicates a higher water level in the coastal ocean as compared with the bay. The elevation of the Station A time series was then adjusted to equal the highest elevation observed at Station D, which occurred on JD 292 (19 October). This adjustment set the Station A elevation at a minimum level and allowed a qualitative comparison with the other stations. It is possible, however, that the actual mean elevation of Station A if leveled to NGVD would be different than plotted.

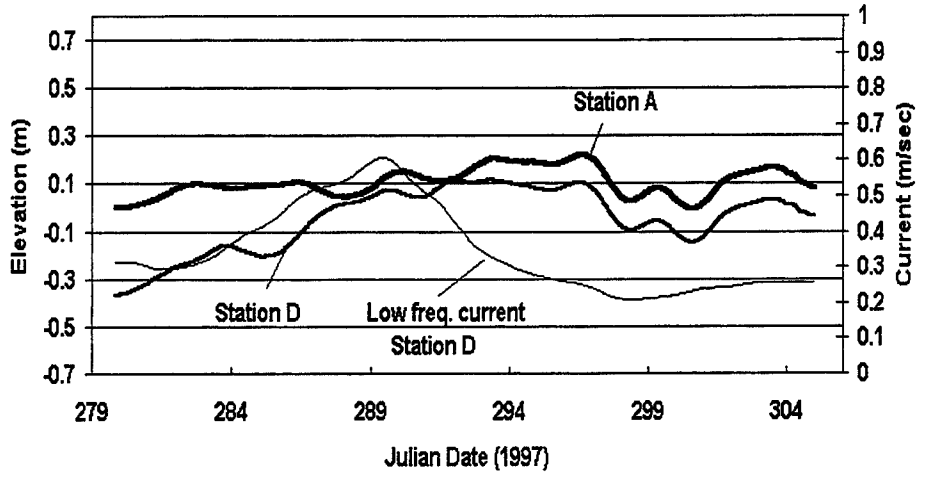

Figure 27. Time series of low-pass filtered water level at Stations A and D and current speed at Station D

The comparison between Station A and Station D shows a similar pattern of subtidal motion at both stations. The higher water elevation observed in the coastal ocean at Station A provided forcing for the subtidal flow directed westward through the inlet. The strongest flow began to develop when the elevation difference between the stations approached 20 cm. After the mean elevation difference decreased to less than 5 cm and remained in the range of 5 to 10 cm, the mean flow speed was reduced.

Figure 28 shows the tidally averaged elevation and subtidal flow observed at Station D for the entire 2-month monitoring session. Two episodes of strong flow reaching speeds of more than 0.4 m/sec occurred. The flood dominant feature of the tides at Ponce Inlet during this time was due largely to the combination of tidal currents and the flood-directed subtidal current.

Figure 29 compares the tidally averaged water elevation observed at Stations D and F during the second half of the monitoring interval when Station F was operational. Figure 29 also shows the subtidal current motion at Station F. The mean water-elevation record at Station F, available for the month of October 1997, is similar to that recorded at Stations A and D (Figures 27 and 29). An increase in mean elevation was recorded at all three stations between JD 280 (7 October) and JD 296 (23 October). The increase at Stations D and F exceeded 0.4 m. During this time, the average elevation of Station D was approximately 10 to 20 cm higher in elevation as compared with Station F. It was during this

time that the subtidal north-to-northwest-directed flow accelerated to a maximum of approximately 0.5 m/sec on JD 286 (13 October). After JD 286 (13 October), the elevation difference between Station D and Station F decreased, coinciding with a decrease in the mean flow at Station F to approximately 0.25 m/sec (Figure 29). The mean elevation records at Stations D and F were similar during the final week of monitoring, but included a slight offset in the mean elevation. The offset was apparently sufficient to keep the subtidal current at Station F propagating north between 0.25 and 0.3 m/sec. Although the comparison of water level is limited, the control on influx into the Ponce Inlet system is the water-level gradient between the ocean and bay. Comparison of water elevations among Stations A, D, and F provides indications of how the water-level gradient changes over time.

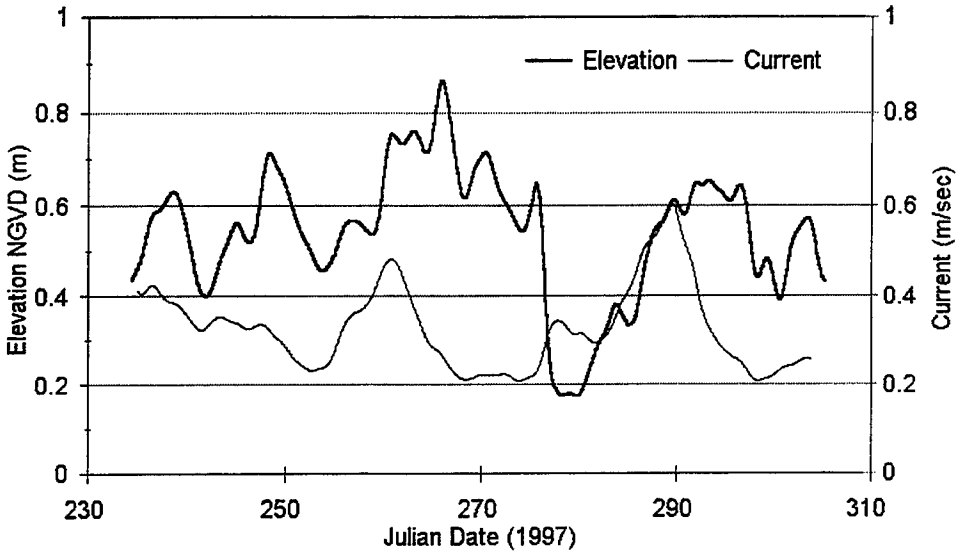

Figure 28. Time series of low-pass filtered water level and current speed at Station D

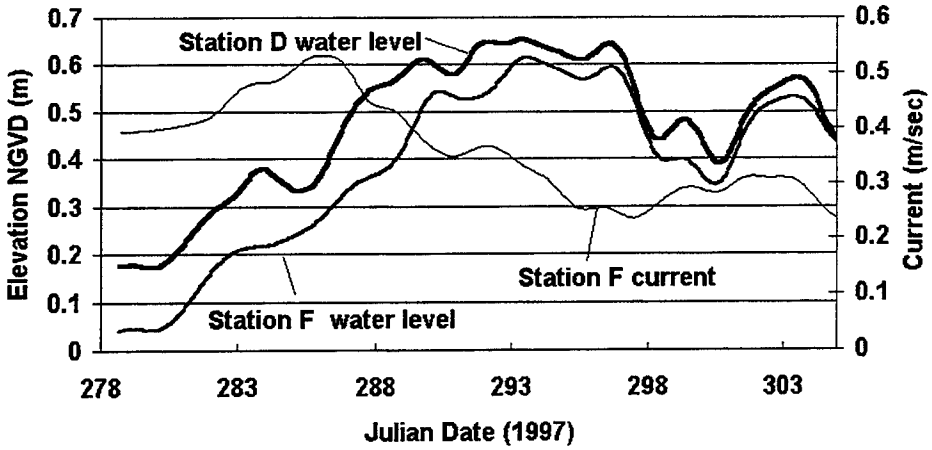

Figure 29. Time series low-pass filtered water level at Stations D and F and current at Station F

Although the mean water level at Station A followed the same pattern as Stations D and F during October, the change in subtidal water elevation was smaller at Station A, amounting to a 25-cm increase in elevation from JD 280 (7 October) to JD 296 (23 October) (Figure 27). However, at the beginning of the October monitoring session, the elevation of Station A was probably 30 cm or more higher than mean water elevation at the interior stations. Thus, a strong subtidal flow developed driving water westward through the inlet, eventually resulting in a net rise of water level at Stations D and F. Future inlet monitoring programs should attempt to level stations situated in the outer inlet or further offshore to quantify spatial differences in water-level motion.

A comparison of the subtidal signals among Stations D, E, and F is shown in Figure 30. The variability of subtidal water level at Station E is less than that at Stations D and F, possibly because of the presence of the Coronado Beach Bridge. The mean water elevation at Station E, located just to the south of the Bridge, remained 40 cm or more below that observed at either Station D or Station F for most of the 2-month monitoring session. The mean water elevation at Station E reached within 3 cm of water elevation at Station D from JD 278 (5 October) to JD 280 (7 October) (Figure 30). During this period the subtidal flow and peak flood current speeds recorded at Station E were among the lowest observed during monitoring.

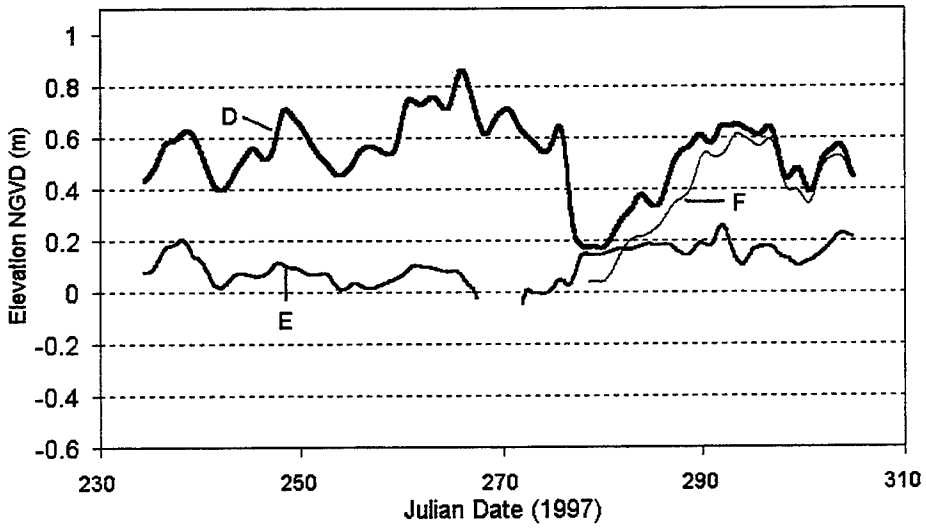

Figure 30. Time series of low-pass filtered water level at back-bay monitoring stations

Tidal Harmonics and Spectra

Spectral analysis and harmonic analysis were applied to time series of water-level data. Energy on specific frequencies can be considered spatially through the Ponce Inlet and back-bay system to investigate tidal wave evolution as it propagates through the inlet. Table 2 lists the amplitude and phase of the M_2 tidal constituent calculated for each of the six stations. Appendix A provides a listing of all 29 tidal constituents computed for each monitoring location, as well as the corresponding phase angles. Appendix A also lists the period of record for

each of the six monitoring stations from which tidal constituents were computed. Overall, there is a decrease in tidal amplitude of approximately 25 percent between Station A on the ebb shoal and Station D in the main conveyance channel of the inlet just west of the inlet throat. The phase of the M_2 tide can both increase and decrease slightly from station to station within the inlet according to the inlet and bay morphology and the localized flow fields.

Table 2
Water Level Amplitude and Phase of the M_2 Tidal Constituent

Station	Location	Amplitude, m	Phase, deg
A	Ebb shoal	0.58	102
B	Inlet channel	0.51	94
C	Inlet channel	0.53	104
D	Conveyance channel	0.45	100
E	Back bay-south	0.26	82
F	Back bay-north	0.30	123

The tidal amplitude in the coastal ocean is represented by Station A, where the M_2 amplitude is 0.58 m. The M_2 amplitude at Station F, located approximately 10 km from Station A, is approximately 50 percent of that at Station A. Station E, located 7 km from Station A (Figure 1), has an M_2 amplitude that is approximately 55 percent of that at the coast. The reduction in amplitude at Stations E and F as compared with that at Station A indicates significant damping of the tidal wave as it propagates through the inlet and back-bay channels. The phase of the M_2 tide at Station F is 123 deg compared with 100 deg at Station A. This phase difference indicates an 0.8-hr time interval for the tidal wave to propagate between Stations A and F. The phase angle at Station E is approximately 20 deg less than the phase angle at Station A, suggesting that the tide at Station E leads the tide at Station A by 0.7 hr. In reality, the tide at Station E would not lead the tidal phase at Station A. The phase calculated for Station E is influenced by flow retardation imposed by the Coronado Beach Bridge (Militello and Zarillo 1999).

A spectrum of the water elevation at Station D is shown in Figure 31. The spectral energy peak near two cycles per day represents the M_2 tide. The spectrum for this station contains near zero energy at the diurnal frequency and a band of energy at the low-frequency end of the spectrum. The low-frequency energy is related to water-level motion at subtidal (period greater than 1 day) time scales. Similarly, Figure 32 shows the semidiurnal spectral peak for water level measured at Station E. However, this spectrum also includes a wide band of energy at lower frequencies, which is probably related to the relatively strong subtidal motion at this station.

Figure 33 shows that the spectrum of Station F data is similar to that of Station D. Here an energy peak occurs at the semidiurnal frequency that is similar in magnitude to the spectrum computed at Station D. Water level at Station F contains energy at the low-frequency end of the spectrum that represents the subtidal motion described for the time series.

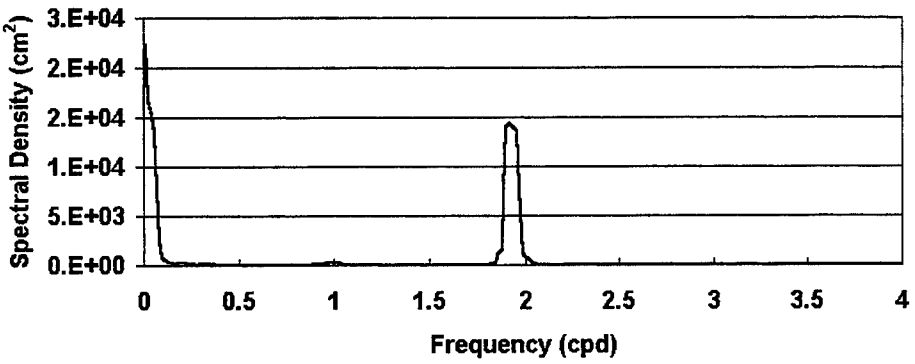

Figure 31. Energy spectrum of water level at Station D

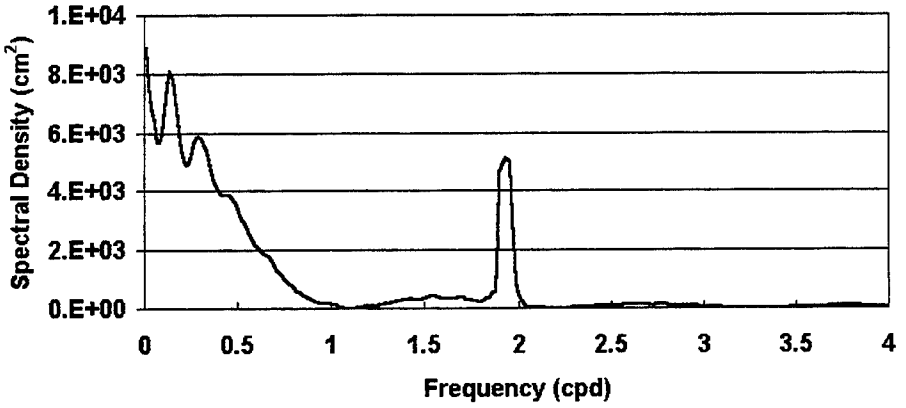

Figure 32. Energy spectrum of water level at Station E

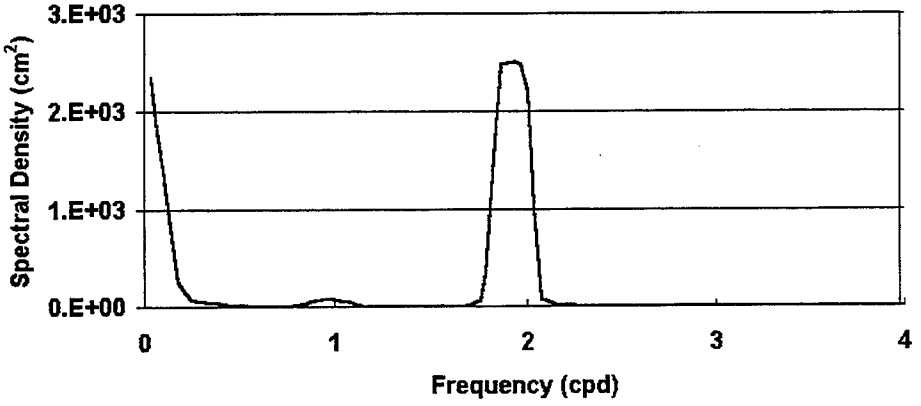

Figure 33. Energy spectrum of water level at Station F

5 Conclusions

The field data-collection campaign at Ponce Inlet successfully acquired water level, current, and wave measurements over a 10-week duration starting on 21 August 1997 and ending on 1 November 1997. Six fixed monitoring stations were deployed at the study site. Three stations in the inlet and on the ebb shoal collected water level, current, and wave data, and the three stations located in the interior collected water level and current data. The overall data-recovery rate was 85 percent.

Observations at the inlet entrance showed that wind waves approached predominantly from the northeast. Spectra for most bursts recorded at Station A (ebb shoal) were somewhat broad banded having secondary energy peaks that may result from wind waves approaching from other directions that cannot be resolved by the puv-type directional wave gauges deployed for this study. Comparison of wave heights among Stations A, B, and C showed that wave energy is strongly attenuated as wind waves move through the inlet entrance. The average significant wave height at Station A was nearly 0.9 m, whereas the average significant wave height at Stations B and C was approximately 0.6 m. An interesting feature of wave records at Stations B and C was the occasional occurrence of significant wave heights of 1 to 2 m. These higher wave heights were infrequent and did not usually persist for more than one burst. All of the spectra calculated for Stations B and C were broad banded, having two or three unequal energy peaks. Most bursts recorded at Station A, although somewhat broad banded, contained one dominant peak. Maximum recorded wave period at all stations was approximately 14 sec or at the imposed low-frequency cutoff. The average wave period at all stations was between 8 and 9 sec. However, the modal or most frequently observed wave period at Station A was approximately 12 sec or about 2 sec shorter as compared with the modal period at Stations B and C.

Comparison of measured water level in the inlet and back bay indicates that the tide is attenuated as it propagates through the system. A maximum observed tidal range of 2.1 m recorded at Station A was reduced to 1.0 m at Station E south of Coronado Beach Bridge. The maximum observed range recorded at Station F was 0.8 m. The energy dissipation is also apparent from the results of the harmonic analysis. The amplitude of the M_2 tidal constituent was reduced by more than 50 percent between Station A on the ebb shoal and Station E. Part of this dissipation is attributed to the resistance of the Coronado Beach Bridge piers on water flow.

Analysis of the data indicated that tidal currents and transient currents, driven by slowly varying exchange between the coastal ocean and back-bay area, interact such that the system was flood dominated during the 2-month-long monitoring interval. Flood dominance is defined by maximum flood-tide current speed exceeding maximum ebb-current speed. Flood dominance was particularly strong in the back-bay areas where tidal currents are weaker as compared with within the inlet. Station F in the Halifax River exhibited strong tidal asymmetry, with the duration and magnitude of the flood flow exceeding that of the ebb flow. During the measurement period, the current at Station E oscillated at tidal frequency, but was directed upstream and rarely reversed to the ebb direction.

The large flood shoal present at Ponce Inlet may indicate the significance of flood dominance in shoal development. Currents measured at the site exhibited a flood-directed bias within the inlet and in the bay channels that varied over time. Superposition of the subtidal flood-directed current with the tide increases peak flood-tide currents and can thereby enhance transport of sand into the back bay where it can be readily deposited.

References

Aubrey, D. G., and Giese, G. S. (1992). *Formation and evolution of multiple tidal inlets*. American Geophysical Union, Washington DC.

Aubrey, D. G., and Weishar, L. (1988). *Hydrodynamics and sediment dynamics of tidal inlets*. Springer-Verlag, New York.

Brown, E. I. (1928). "Inlets on sandy coasts." *Proceedings of the American Society of Civil Engineers*, Vol LIV, 505-553.

FitzGerald, D. M. (1984). "Interactions between the ebb-tidal delta and landward shoreline: Price Inlet, South Carolina," *Journal of Sedimentary Petrology* 54, 1303-1318.

Harkins, G. S., Puckette, P., and Dorrell, C. (1997). "Physical model studies of Ponce de Leon Inlet, Florida," Technical Report CHL-97-23, U.S. Army Engineer Waterways Experiment Station, Vicksburg, MS.

Hayes, M. O. (1979). "Barrier island morphology as a function of tidal and wave regime." *Barrier islands from the Gulf of St. Lawrence to the Gulf of Mexico*. S. P. Leatherman, ed., Academic Press, New York, 1-27.

Jones, C. P., and Mehta, A. J. (1978). "Ponce de Leon Inlet, glossary of inlets Report #6," Florida Sea Grant Program, FL.

Keulegan, G. H. (1951). "Third progress report on tidal flow in entrances: Water level fluctuations of basins in communication with seas," Report No. 1146, National Bureau of Standards, Washington, DC.

King, D. B., Jr. (1974). "The dynamics of inlets and bays," Technical Report No. 22, Coastal and Oceanographic Engineering Laboratory, University of Florida, Gainsville, FL.

King, D. B., Smith, J. M., Militello, A., Stauble, D. S., and Waller, T. N. (1999). "Ponce de Leon Inlet, Florida, site investigation. Report 1: Selected portions of long-term measurements, 1995-1997," Technical Report CHL-99-1, U.S. Army Engineer Waterways Experiment Station, Vicksburg, MS.

Militello, A., and Zarillo, G. A. (1999). "Tidal motion in a complex inlet and bay system, Ponce de Leon Inlet, Florida," *Journal of Coastal Research* (in press).

Ozoy, E. (1977). "Flow and mass transport in the vicinity of tidal inlets," Technical Report TR-036, Coastal and Oceanographic Engineering Laboratory, University of Florida, Gainsville, FL.

Parthenaides, E., and Purpura, J. A. (1972). "Coastline changes near a tidal inlet." *Proceedings of the Thirteenth Coastal Engineering Conference.* ASCE, 843-863.

Purpura, J. A. (1977). "Performance of a jetty-weir inlet improvement plan." *Proceedings of Coastal Sediments 1977.* ASCE, 330-349.

Taylor, R. B., Hull, T. J., Srinivas, R., and Dompe, P. E. (1996). "Ponce de Leon Inlet feasibility study, numerical modeling and shoaling analysis, Volume I," Taylor Engineering, Inc., Jacksonville, FL.

van de Kreeke, J. (1986). "Hydrodynamics of tidal inlets." *Lecture notes on coastal and estuarine studies.* Springer-Verlag, New York, 1-21.

Zarillo, G. A., Ward, L. G., and Hayes, M. O. (1985). *An illustrated history of tidal inlet changes in south carolina.* South Carolina Sea Grant Consortium.

Zarillo, G. A., and Liu, J. T. (1990). "Shoreface building and maintenance: The role of tidal inlets," *Journal of Coastal Research*, Special Issue No. (9), 911-935.

Appendix A
Tidal-Constituent Amplitudes for Water Level at the Six Instrument Locations

This appendix provides tidal constituents calculated for water-level data collected during the short-term field campaign at the Ponce Inlet study site. Tidal constituents were calculated by application of standard National Ocean Service harmonic analysis procedures. Twenty-nine-day segments of data were analyzed. For stations having more than one reliable 29-day segment, the harmonic analysis was conducted on each segment, then vector averaged to give a composite result. Table A1 gives the dates over which the harmonic analysis was conducted for each station. The start date defines the day on which the analysis started, and the end date specifies the day through which the analysis ran. Constituents presented in Tables A2 through A7 are representative of the 29-day intervals during which the data were collected. The tidal amplitudes and phases may differ from those collected at other times because of seasonal and longer period variations in hydrodynamic properties of the coastal ocean.

Table A1
Dates of Harmonic Analysis Applied to Water-Level Measurements

Station	Start Date, 1997	End Date, 1997
A	03 October	31 October
B	22 August	19 September
	29 August	25 September
C	22 August	19 September
	29 August	25 September
D	22 August	19 September
	29 August	25 September
	04 September	02 October
	11 September	09 October
	18 September	16 October
	25 September	23 October
	02 October	30 October
E	22 August	19 September
	29 August	25 September
	04 September	02 October
	11 September	09 October
	18 September	16 October
	25 September	23 October
	02 October	30 October
F	04 October	01 November

Table A2
Harmonic Constituents for Station A

Tidal Constituent	Amplitude, m	Local Phase, deg
M2	0.59	102
S2	0.10	118
N2	0.16	71
K1	0.08	46
M4	0.01	300
O1	0.07	69
M6	0.00	239
S4	0.00	61
S6	0.00	227
M8	0.00	257
MK3	0.00	313
MN4	0.00	274
MS4	0.01	275
MSF	0.03	113
NU2	0.02	95
MU2	0.01	87
2N2	0.02	85
OO1	0.00	23
LAM2	0.00	305
M1	0.01	58
J1	0.01	35
RHO1	0.00	79
Q1	0.01	81
T2	0.01	117
R2	0.00	119
2Q1	0.00	92
P1	0.03	48
L2	0.02	111
K2	0.03	120

Table A3
Harmonic Constituents for Station B

Tidal Constituent	Amplitude, m	Local Phase, deg
M2	0.51	91
S2	0.09	115
N2	0.13	62
K1	0.08	73
M4	0.01	262
O1	0.06	79
M6	0.00	294
S4	0.01	338
S6	0.00	330
M8	0.00	26
MK3	0.00	34
MN4	0.00	299
MS4	0.01	236
MSF	0.05	94
NU2	0.02	80
MU2	0.01	67
2N2	0.01	65
OO1	0.00	68
LAM2	0.00	311
M1	0.00	76
J1	0.01	71
RHO1	0.00	81
Q1	0.01	81
T2	0.01	114
R2	0.00	116
2Q1	0.00	84
P1	0.03	74
L2	0.01	104
K2	0.02	117

Table A4
Harmonic Constituents for Station C

Tidal Constituent	Amplitude, m	Local Phase, deg
M2	0.53	105
S2	0.09	130
N2	0.13	76
K1	0.08	80
M4	0.01	288
O1	0.06	85
M6	0.00	347
S4	0.01	10
S6	0.00	7
M8	0.00	106
MK3	0.00	52
MN4	0.01	325
MS4	0.01	265
MSF	0.06	94
NU2	0.02	93
MU2	0.01	80
2N2	0.01	79
OO1	0.00	76
LAM2	0.00	304
M1	0.00	83
J1	0.01	79
RHO1	0.00	87
Q1	0.01	87
T2	0.01	129
R2	0.00	130
2Q1	0.00	89
P1	0.03	81
L2	0.01	118
K2	0.03	132

Table A5
Harmonic Constituents for Station D

Tidal Constituent	Amplitude, m	Local Phase, deg
M2	0.45	100
S2	0.09	126
N2	0.14	70
K1	0.06	63
M4	0.01	308
O1	0.07	68
M6	0.01	31
S4	0.01	40
S6	0.00	14
M8	0.00	28
MK3	0.00	138
MN4	0.00	305
MS4	0.01	272
MSF	0.06	86
NU2	0.02	89
MU2	0.01	75
2N2	0.01	73
OO1	0.00	61
LAM2	0.00	308
M1	0.00	66
J1	0.00	62
RHO1	0.00	70
Q1	0.01	70
T2	0.00	125
R2	0.00	127
2Q1	0.00	72
P1	0.02	63
L2	0.01	114
K2	0.02	128

Table A6
Harmonic Constituents for Station E

Tidal Constituent	Amplitude, m	Local Phase, deg
M2	0.27	82
S2	0.05	109
N2	0.08	70
K1	0.03	43
M4	0.00	268
O1	0.02	40
M6	0.01	83
S4	0.00	286
S6	0.00	38
M8	0.00	324
MK3	0.01	254
MN4	0.00	182
MS4	0.00	289
MSF	0.07	69
NU2	0.01	70
MU2	0.01	54
2N2	0.01	52
OO1	0.00	34
LAM2	0.00	317
M1	0.00	38
J1	0.00	35
RHO1	0.00	40
Q1	0.00	41
T2	0.00	108
R2	0.00	110
2Q1	0.00	42
P1	0.01	43
L2	0.01	96
K2	0.01	112

Table A7
Harmonic Constituents for Station F

Tidal Constituent	Amplitude, m	Local Phase, deg
M2	0.31	124
S2	0.05	139
N2	0.07	101
K1	0.05	55
M4	0.00	63
O1	0.04	89
M6	0.01	108
S4	0.00	56
S6	0.00	102
M8	0.00	127
MK3	0.00	336
MN4	0.00	31
MS4	0.00	251
MSF	0.05	76
NU2	0.01	116
MU2	0.01	108
2N2	0.01	107
OO1	0.00	20
LAM2	0.00	294
M1	0.00	72
J1	0.00	38
RHO1	0.00	104
Q1	0.01	106
T2	0.00	138
R2	0.00	140
2Q1	0.00	123
P1	0.02	57
L2	0.01	132
K2	0.01	140

Appendix B
Conversion Table for Calendar Day and Julian Day

This appendix provides a table for converting between calendar day and Julian day. Add 1 to italicized values during a leap year.

Table B1
Conversion Table for Calendar Day and Julian Day

Day of Month	Jan	Feb	Mar	Apr	May	Jun	Jul	Aug	Sep	Oct	Nov	Dec
1	1	32	*60*	*91*	*121*	*152*	*182*	*213*	*244*	*274*	*305*	*335*
2	2	33	*61*	*92*	*122*	*153*	*183*	*214*	*245*	*275*	*306*	*336*
3	3	34	*62*	*93*	*123*	*154*	*184*	*215*	*246*	*276*	*307*	*337*
4	4	35	*63*	*94*	*124*	*155*	*185*	*216*	*247*	*277*	*308*	*338*
5	5	36	*64*	*95*	*125*	*156*	*186*	*217*	*248*	*278*	*309*	*339*
6	6	37	*65*	*96*	*126*	*157*	*187*	*218*	*249*	*279*	*310*	*340*
7	7	38	*66*	*97*	*127*	*158*	*188*	*219*	*250*	*280*	*311*	*341*
8	8	39	*67*	*98*	*128*	*159*	*189*	*220*	*251*	*281*	*312*	*342*
9	9	40	*68*	*99*	*129*	*160*	*190*	*221*	*252*	*282*	*313*	*343*
10	10	41	*69*	*100*	*130*	*161*	*191*	*222*	*253*	*283*	*314*	*344*
11	11	42	*70*	*101*	*131*	*162*	*192*	*223*	*254*	*284*	*315*	*345*
12	12	43	*71*	*102*	*132*	*163*	*193*	*224*	*255*	*285*	*316*	*346*
13	13	44	*72*	*103*	*133*	*164*	*194*	*225*	*256*	*286*	*317*	*347*
14	14	45	*73*	*104*	*134*	*165*	*195*	*226*	*257*	*287*	*318*	*348*
15	15	46	*74*	*105*	*135*	*166*	*196*	*227*	*258*	*288*	*319*	*349*
16	16	47	*75*	*106*	*136*	*167*	*197*	*228*	*259*	*289*	*320*	*350*
17	17	48	*76*	*107*	*137*	*168*	*198*	*229*	*260*	*290*	*321*	*351*
18	18	49	*77*	*108*	*138*	*169*	*199*	*230*	*261*	*291*	*322*	*352*
19	19	50	*78*	*109*	*139*	*170*	*200*	*231*	*262*	*292*	*323*	*353*
20	20	51	*79*	*110*	*140*	*171*	*201*	*232*	*263*	*293*	*324*	*354*
21	21	52	*80*	*111*	*141*	*172*	*202*	*233*	*264*	*294*	*325*	*355*
22	22	53	*81*	*112*	*142*	*173*	*203*	*234*	*265*	*295*	*326*	*356*
23	23	54	*82*	*113*	*143*	*174*	*204*	*235*	*266*	*296*	*327*	*357*
24	24	55	*83*	*114*	*144*	*175*	*205*	*236*	*267*	*297*	*328*	*358*
25	25	56	*84*	*115*	*145*	*176*	*206*	*237*	*268*	*298*	*329*	*359*
26	26	57	*85*	*116*	*146*	*177*	*207*	*238*	*269*	*299*	*330*	*360*
27	27	58	*86*	*117*	*147*	*178*	*208*	*239*	*270*	*300*	*331*	*361*
28	28	59	*87*	*118*	*148*	*179*	*209*	*240*	*271*	*301*	*332*	*362*
29	29	60*	*88*	*119*	*149*	*180*	*210*	*241*	*272*	*302*	*333*	*363*
30	30		*89*	*120*	*150*	*181*	*211*	*242*	*273*	*303*	*334*	*364*
31	31		*90*		*151*		*212*	*243*		*304*		*365*

* Leap year only

REPORT DOCUMENTATION PAGE

Form Approved
OMB No. 0704-0188

1. AGENCY USE ONLY *(Leave blank)*

2. REPORT DATE
March 1999

3. REPORT TYPE AND DATES COVERED
Report 2 of a series

4. TITLE AND SUBTITLE
Ponce de Leon Inlet, Florida, Site Investigation; Report 2, Inlet Hydrodynamics: Monitoring and Interpretation of Physical Processes

5. FUNDING NUMBERS

6. AUTHOR(S)
Gary A. Zarillo, Adele Militello

7. PERFORMING ORGANIZATION NAME(S) AND ADDRESS(ES)
Division of Marine and Environmental Systems, Florida Institute of Technology,
150 W. University Boulevard, Melbourne, FL 32901;
U.S. Army Engineer Waterways Experiment Station
3909 Halls Ferry Road, Vicksburg, MS 39180-6199

8. PERFORMING ORGANIZATION REPORT NUMBER
Technical Report CHL-99-1

9. SPONSORING/MONITORING AGENCY NAME(S) AND ADDRESS(ES)
U.S. Army Corps of Engineers
Washington, DC 20314-1000

10. SPONSORING/MONITORING AGENCY REPORT NUMBER

11. SUPPLEMENTARY NOTES
Available from National Technical Information Service, 5285 Port Royal Road, Springfield, VA 22161.

12a. DISTRIBUTION/AVAILABILITY STATEMENT
Approved for public release; distribution is unlimited.

12b. DISTRIBUTION CODE

13. ABSTRACT *(Maximum 200 words)*

Field-data collection was conducted at Ponce de Leon Inlet, Florida, from 21 August 1997 through 1 November 1997 to measure wind waves, water level, and current. Six monitoring stations were deployed, one on the ebb shoal, three within the inlet, and two in the back bay north and south of the inlet. Wave data were collected in the inlet and on the ebb shoal, while water level and current were measured at all stations.

During the measurement interval, waves approached predominantly from the northeast. Significant wave heights were greatest over the ebb shoal (average 0.9 m) and were reduced at the inlet stations (average of 0.6 m). Average wave period was between 8 and 9 sec, and maximum period was 14 sec.

The tide at all inlet and bay stations exhibited flood dominance and exhibited net landward-directed flow. Flood dominance was strongly exhibited in the back bay and at one interior station south of the inlet; the flow rarely changed from flood to ebb. Tidal attenuation was greatest at measurement locations far from the inlet. Comparison of M_2 amplitudes of water level suggests that the Coronado Beach Bridge, located south of the inlet, may be responsible for strong dissipation of tidal energy.

14. SUBJECT TERMS
Flood dominance
Tidal attenuation
Tidal current
Tidal inlet
Wind waves

15. NUMBER OF PAGES
39

16. PRICE CODE

17. SECURITY CLASSIFICATION OF REPORT	18. SECURITY CLASSIFICATION OF THIS PAGE	19. SECURITY CLASSIFICATION OF ABSTRACT	20. LIMITATION OF ABSTRACT
UNCLASSIFIED	UNCLASSIFIED		